https://doi.org/10.1016/j.matchemphys.2016.06.075

Laser fabrication of W-reinforced Cu layers: I. Corrosion behavior in 3.5% NaCl solution and synthetic acid rain

P.K. Wong[a], C.T. Kwok[a,b,*], H.C. Man[c], D. Guo[a]

[a] Department of Electromechanical Engineering, University of Macau, China

[a,b] Institute of Applied Physics and Materials Engineering, University of Macau, China

[c] Department of Industrial and Systems Engineering, The Hong Kong Polytechnic University, Hong Kong, China

[*] Corresponding author: Tel.: 853-8822-4459; Fax: 853-8822-2426;

E-mail address: fstctk@umac.mo

Abstract

Surface modification of cp Cu with W was achieved by using a high power diode laser (HPDL) resulting in a microstructure of micron-sized W particles in a Cu matrix. In both 3.5 wt% NaCl solution and synthetic acid rain (SAR), the laser-fabricated specimens possess lower corrosion current density (I_{corr}) than that of cp Cu despite the active shift in open-circuit potential (*OCP*). Although Cu is cathodic to W in 3.5 wt% NaCl solution, the Cu phase in the laser-fabricated specimens dominantly dissolves during the immersion test. This anomalous observation is possible because the *OCP* values of the laser-fabricated specimens, cp Cu and cp W are quite near to each other, while the anodic and cathodic current densities are all not negligible for the Cu and W phases at OCP. As the anodic current density of the Cu phase is greater than anodic current density of the W phase, the Cu phase corrodes more quickly than the W phase. For the laser-fabricated specimens immersed in SAR, the Cu phase is anodic and is

selectively attacked while the W phase is passive due to the formation of WO_3.

Keywords: alloys; coatings; SEM; corrosion

1. Introduction

Copper (Cu) is an excellent electric contact material due to its high electrical and thermal conductivities, high ductility, ease of fabrication and reasonable affordability. However, its major drawbacks are low hardness, low wear resistance, and susceptibility to corrosion in chloride-containing media. Tungsten-copper (W-Cu) composites combine the high hardness, high-temperature strength and excellent resistance to burning (by sparks and electric arcs) of W and the merits of Cu [1], leading to a wide range of applications including arcing contacts in voltage breakers for transmission and distribution of electrical power, erosion and arcing resistant electrodes for electric discharge machining and welding, heat sinks of electronic devices and special-purpose materials for rockets and missiles. Conventionally, W-Cu composites are commonly produced by infiltration of a porous sintered W piece by liquid Cu. Due to the limited mutual solubility, poor wettability, large differences in melting point and coefficient of thermal expansion of Cu and W, defects including pores, Cu lakes and W agglomerates are often formed in the structure [2–4]. Such defects would contribute to low corrosion resistance and hence significantly limit their application in corrosive environments.

Laser surface modification is a technique for modifying the near-surface region of materials without changing the bulk properties. A laser is a clean energy source which allows a wide range of surface modification via melting of substrate and/or coating materials through the absorption of the laser energy. It is especially suitable for modifying the surface of components suffering from corrosion and wear at

localized regions while retaining the bulk properties, thus obtaining optimal combination of surface and bulk properties at affordable cost. It was reported that the surface properties of engineering alloys such as hardness [5-9], resistances to corrosion [10-13], erosion and abrasion [9], wear [8,11-13], oxidation [14-17] and fatigue crack growth [20] were significantly improved by laser surface modification. Particularly, laser surface modification of Cu is extremely challenging due to its high reflectivity to infra-red light and high thermal conductivity. As a result very few studies on laser surface modification of Cu were reported in the literature. Hirose and Kobayashi firstly reported that Cu-Cr alloyed layers of thickness 100 to 200 μm were produced by laser surface modification of Cr powder beds or a plasma-sprayed Cr coating on Cu substrate with a 2.5-kW CO_2 laser (beam diameter of 1.2 mm, traverse speed of 0.33 mm/s, He shielding) for improving hardness and wear resistance at elevated temperatures without sacrificing its electrical properties [8]. The Cr content of the modified layers was approximately 20 wt%. Due to the limited solid solubility between Cr and Cu, laser surface modification causes pure Cr particles to be precipitated and finely dispersed upon rapid cooling. The modified layers had higher hardness (120 HV) than that of pure Cu (60-70 HV) at room temperature due to the presence of dispersed Cr particles. Moreover, the hardness of the modified layers was 3-4 times that of pure Cu at 873 K. Similar work was reported by Majumdar and Manna who attempted laser treatment of Cu substrate with the incorporation Cr for improving abrasion and erosion resistances using a CW CO_2 laser [9,21]. The modified zone consists of dispersed Cr-rich particles in a Cu-rich solid solution and is consistent with the findings of Hirose and Kobayashi. The laser fabricated Cu-Cr layer possesses 2–3 times increase in hardness and the wear resistance was significantly improved. Laser remelting of a powder mixture 48Cu-48Cr-4Fe (wt%) was studied by Geng and his co-workers [17]. After remelting, a refined spherical Cr

phase was uniformly dispersed in the Cu-rich matrix. Increased compactness and refined microstructure of the remelted alloy led to increased hardness, wear resistance and a reduced friction coefficient as compared with the base material. Laser surface modification of cp Cu with preplaced Ti powder using a high power diode laser has been reported by Wong et al [13]. The Ti-alloyed Cu possesses lower corrosion current density than that of cp Cu. Particularly, the laser-modified specimen with 85 wt% Ti shows the highest corrosion resistance, that is, about 150 times that of cp Cu and very close to that of cp Ti. Improvement of corrosion resistance is attributed to the presence of Ti in the intermetallic and metallic phases for forming the protective oxide.

Studies on selective laser melting (SLM) and direct metal laser sintering (DMLS) of bulk W-Cu composites were reported [22,23]. Li and his coworkers reported that SLM of W-10wt%Cu composite with a 100-W CW/modulated fibre laser resulted in complete melting of Cu but without melting of W [22]. The binder (Cu) was molten and infiltrated the W particles, then solidified as a continuous solid phase with uniformly distributed W particles in the Cu matrix. On the other hand, Gu and his coworkers reported that DMLS of a composite system consisting of 40 wt% submicron W-20Cu powder and 60 wt% micron Cu powder was performed with a 2-kW CW CO_2 laser to produce a series of regularly shaped W-rim/Cu-core structures [23]. The formation of the W-rim was attributed to the combined action of the clockwise thermal Marangoni flow and the counterclockwise solutal one, which was induced by temperature gradient or chemical concentration at a solid/liquid interface. The repulsive forces between the W particles in the Cu liquid prevented the W-rim from merging, thereby forming the Cu-core after solidification. The difference in resultant microstructure by SLM and DMLS is ascribed to different processing routes. In both studies, only the microstructural evolution of the bulk W-Cu composites was

addressed. On the other hand, the feasibility of depositing W-Cu composite overlays on bronze substrate by laser cladding was explored by Wang and Xue [24]. Metallographic analysis of the composite coatings revealed that coalescence and separation of the W particles occurred more easily for the fine W powders than for the coarse ones due to poor wetting behavior.

Levy and Chang conducted anodic polarization studies on pure W and different heavy W composites fabricated by sintering, in 0.1 M NaCl solution at pH 4, 9 and 12 and immersion tests in 5% NaCl solution [25]. A general increase in corrosion rates with increasing pH was observed and composites containing Cu had the highest corrosion rates. Both general dissolution and localized attack at grain boundaries were observed but the evolution of corrosion is unknown. On the other hand, Ogundipean and his co-workers studied the corrosion behaviors of five sintered heavy W composites by immersion test in distilled water and by acid wet–dry cycle test at pH 4 [26]. A general trend of binder phase corrosion was observed in four alloys (W-7wt%Ni-3wt%Fe, W-1.8wt%Ni-1.2wt%Fe, W-4.7wt%Ni-2.3wt%Co and W-4.5wt%Ni-1.5wt%Fe-1.0wt%Co) while W-5.1wt%Cu showed significant W phase corrosion.–The release of W as well as other elements is due to galvanic corrosion resulting from the difference in electrode potential between the W phase and the binder phase in all composites studied. To exploit the feasibility of the laser-fabricated Cu-W coatings (without porosity and lower W contents, i.e. 55 to 60 wt% W) for electrical contact applications, their performance in hostile environments was investigated in the present study. The electrochemical corrosion behavior and evolution of corrosion in 3.5 wt% NaCl solution and synthetic acid rain (SAR) at 25 ^{o}C by immersion tests were investigated in Part I while the electrical sliding wear behavior in air and SAR will be reported in Part II [27].

2. Experimental details

2.1 Specimens preparation

Rectangular plates of commercial pure copper (cp Cu) with dimensions of 22 mm x 19 mm x 6.3 mm were ground with 80-grit SiC paper to remove surface oxide and increase roughness for adhesion with the blend powders (90 wt% W and 10 wt% Cu). The Cu plates were then ultrasonically cleaned in ethanol and then washed in distilled water. Fig. 1 shows the morphologies of the W and Cu powders. The W and Cu particles show a polygonal shape which will facilitate more surface area for laser absorption during laser surface modification. The average particle size of W and Cu powders is 20 and 10 μm respectively. The blend powders were mixed with 4 wt% polyvinyl alcohol, which acted as a binder. The slurry of the powders was then pasted onto the surface of cp Cu by a paintbrush and the thickness of the preplaced layer (d) was controlled to 0.1 mm approximately. The preplaced powders on the Cu substrate can circumvent its high reflectivity [9,21,28] and improve laser absorption. The specimen was preheated with a heating plate to a temperature of 150 ^{o}C for reducing residual stress level [29] and also for improving laser absorption, which is temperature dependent. Laser surface modification was then carried out using a 2.3-kW CW HPDL module (Laserline, LDM 1000-1000) at powers of 1.8 and 2 kW, a beam diameter of 2 mm and scanning speed of 40 mm/s. HPDL possesses the advantage of a short wavelength (990 nm) which is better absorbed by metals. Argon gas flowing at a rate of 15 L/min was used as the shielding gas to avoid oxidation during the process. The laser-fabricated surface was accomplished by overlapping adjacent parallel melt tracks with 50% overlapping. Considering that the preplaced layer contained 90 wt% W, the dilution ratio (DR) showing the degree of dilution of W the coatings is calculated as follows:

$$DR = 0.9 \times \left(1 - \frac{d}{D}\right) \qquad (1)$$

where d is thickness of the preplaced layer and D is thickness of the laser-fabricated layer. Note that the DR is for W. Since the preplaced powder contain 90 wt% W and 10% wt% Cu, a factor of 0.9 is used. The values of D and DR are shown in Table 2. According to this definition, the higher is the DR value, the higher is the degree of dilution. Surface of the specimens were ground with 400-grit SiC paper to remove surface oxide and then ultrasonically cleaned in ethanol followed by washing in distilled water for polarization study and immersion test.

2.2 Microstructural analysis

The laser-fabricated specimens were cut along the transverse cross-section of the laser-fabricated layers, followed by mounting with epoxy, grinding with SiC papers up to 800-grit, polishing with 1 μm diamond paste, and lastly etching with acidified ferric chloride solution (25 g $FeCl_3$, 25 ml HCl and 100 ml H_2O). Microstructural examination was then conducted by scanning-electron microscopy (SEM, Hitachi S-3400N). Phase identification was conducted using X-ray diffractometer (XRD, Rigaku MiniFlex 600) with CuKα radiation operating at 40 kV and 15 mA and the scan rate was 0.1 °/s. The XRD patterns of the specimens before and after immersion tests were taken from the top surface.

2.3 Electrochemical measurement

Potentiodynamic polarization tests of the laser-fabricated specimens, cp Cu and cp W were performed in stagnant 3.5 wt% NaCl solution and synthetic acid rain (SAR), open to air, at 25±1 ^{o}C using a potentiostat (PAR VersastatII) conforming to ASTM Standard G5-92 [30]. In order to simulate the acid rain water, SAR was prepared according to the rain composition obtained by The Macao Meteorological and Geophysical Bureau (SMG) in 2012 [31]. The composition of the SAR used in

the present study contains: SO_4^{2-} 31 mg/L, NO_3^- 11 mg/L, Cl^- 27.3 mg/L, Na^+ 27.3 mg/L, Ca^{2+} 5.5 mg/L at pH 3.5. For electrochemical measurements, all potentials were measured with respect to a saturated calomel electrode (SCE, +0.244V versus SHE at 25 ^oC) as the reference electrode. Two parallel graphite rods served as the counter electrode for current measurement. An initial delay of 120 minutes prior to polarization was adopted for the specimen to reach a steady-state condition at open-circuit potential (*OCP*). After that, the potential was increased at a rate of 0.167 mV/s, starting from 0.2 V_{SCE} below the OCP. From the polarization curve, the corrosion current density (I_{corr}) was extracted by Tafel extrapolation. Three replicate samples were used in the polarization test for each type of specimens.

2.4 Immersion test

In order to investigate the evolution of corrosion of the laser-fabricated specimens, cp Cu and cp W and in 3.5 wt% NaCl solution and SAR at 25 ^oC, immersion tests were conducted. After being polished with 1-μm diamond paste, specimens mounted by epoxy exposing an area of 1-cm^2 were put into individual beakers with 500-mL 3.5 wt% NaCl solution and SAR keeping in a water bath at 25 ^oC. They were intermittently taken out at the first, third, sixth and ninth weeks and then ultrasonically cleaned in ethanol and dried for further morphological observation by SEM.

3. Results and Discussion

3.1 Microstructure

Owing to the higher laser absorptivity of W [32], it was easier to heat up the surface and subsequently transfer the heat to the Cu substrate. The temperature achieved was only high enough to melt Cu while W was infiltrated in the molten Cu. The laser-fabricated specimens are designated as ‘LA-W-Cu-pXX’ where pXX

represents the power in kW. The transverse cross-section and microstructure of the laser-fabricated specimens LA-W-Cu-p1.8 and LA-W-Cu-p2 are shown in Figs. 2 and 3 respectively. The thicknesses (*D*) of the laser-fabricated layers are depicted in Table 1. Strong metallurgical bond was formed between the laser-fabricated layers and the Cu substrate. The laser-fabricated layers were free of cracks and porosities. This shows that the convection flows were sufficient to eliminate the porosities in the preplaced layer [33]. After rapid solidification, an ensuing microstructure containing two distinct phases, i.e. the bcc W particulate phase and fcc Cu binder phase were detected by XRD as shown in Fig. 4. The microstructure of the laser-fabricated specimens consists of micron-sized W particles dispersed in a Cu matrix (Figs. 2b and 3b). The W phase is essentially pure W, and is surrounded by the Cu binder phase. A surface with non-uniform sized W particles (average size of 0.5 to 20 μm) can be observed from the cross-section of the laser-fabricated specimen LA-W-Cu-p1.8 (Fig. 2b). For LA-W-Cu-p2, larger W particles with average size of 30 μm are uniformly dispersed in the Cu matrix as shown in Fig. 3b. A contiguous microstructure with contacts between the W particles can be also observed. From Fig. 3c, W is undiluted because of the large difference in melting temperature and the mutual insolubility of W and Cu. EDX line scan across the two phases reveals that the brighter contrast region is the W phase while the darker one is the Cu phase. By image and compositional analyses, the W content in the laser-fabricated layers is about 55 and 60 wt% for LA-W-Cu-p1.8 and LA-W-Cu-p2 respectively. Lower W content is observed in LA-W-Cu-p1.8 because the laser power of 1.8 kW is not high enough for the W phase to infiltrate completely in the Cu binder. Some W particles were not bonded to the laser-fabricated layer and lost. It is not surprising that the W content of LA-W-Cu-p1.8 is found to be lower than expected and inconsistent with the estimated lower DR, i.e. lower degree of dilution as shown in Table 2.

3.2 Electrochemical behavior

The plots of *OCP* against time and potentiodynamic polarization curves of the laser-fabricated specimens, cp Cu and cp W in 3.5 wt% NaCl solution and SAR (open to air) at 25 ^{o}C are shown in Figs. 5 and 6 respectively. The steady *OCP* and corrosion current densities (I_{corr}) are summarized in Table 2. Generally, the *OCP* values for all specimens in 3.5 wt% NaCl solution are more active than those in the SAR. From Figs. 5a and 6a, cp W is the most active, cp Cu is the most noble and the *OCP* values for the laser-fabricated specimens are in-between in both media. It is consistent with the galvanic series of metals and alloys [34]. The polarization curve of cp W reveals that the electrochemical behavior of W differs substantially from those of cp Cu and the laser-fabricated specimens in both media as shown in Figs. 5b and 6b. cp W undergoes an active to passive transition while cp Cu and the laser-fabricated specimens do not. None of the polarization curves show a transpassive region. According to the values of I_{corr} shown in Table 2, the ranking of corrosion resistance of the specimens is:

cp W > LA-W-Cu-p2 > LA-W-Cu-p1.8 > cp Cu

Among the specimens, cp W is found to be the most corrosion resistant while Cu exhibits the lowest corrosion resistance in both media. All laser-fabricated specimens have lower I_{corr} than that of cp Cu despite the active shift in *OCP*. The I_{corr} of LA-W-Cu-p2 is lower than that of LA-W-Cu-p1.8. I_{corr} decreases (i.e. corrosion resistance increases) with the increase in W content of the laser-fabricated specimens.

3.2.1 In 3.5 wt% NaCl solution

The Pourbaix diagrams for Cu and W in water at 25 ^{o}C [35] provide a thermodynamic basis for explaining the phenomena of dissolution and oxide

formation in aqueous solutions under different electrochemical conditions. At pH 7, W readily dissolves in water as tungstate (WO_4^{2-}) at a rate dependent on its potential:

$$W + 4H_2O \rightarrow WO_4^{2-} + 8H^+ + 6e^- \qquad (2)$$

It shows that the tungstic ion (WO_4^{2-}) is stable at *OCP* (-0.444 V_{SCE}) and the corrosion reaction is possible. On the other hand, the cathodic reaction is reduction of water and oxygen given by

$$O_2 + 4H_2O + 4e^- \rightarrow 4OH^- \qquad (3)$$

The strong effect of O_2 content in the electrolyte suggests that the reduction of O_2 is the dominant cathodic reaction given by (3). Another possible chemical reaction is the dissolution of tungsten oxide (WO_3). Lillard *et al.* showed that W exposed to air has a native oxide WO_3 through surface-enhanced-Raman spectroscopy [36]. It is suggested that WO_3 dissolves at the cell equilibrium potential and pH 7 as given by (4).

$$WO_3 + 4H_2O \rightarrow WO_4^{2-} + 2H^+ \qquad (4)$$

Therefore, even if a native oxide layer exists initially on the W surface that inhibits dissolution, eventually the oxide will dissolve and expose the W surface.

In 3.5 wt% NaCl solution (pH 7), the anodic current density of cp W remains at a low value and becomes constant above +0.125 V_{SCE} (showing passivity) as compared with cp Cu and the laser-fabricated specimens. Polarization curves of the laser-fabricated specimens are very similar except that the *OCP* of LA-W-Cu-p1.8 (-0.303 V_{SCE}) is slightly nobler than that of LA-W-Cu-p2 (-0.324 V_{SCE}) owing to the existence of the nobler Cu phase. Distinct 'knees' are observed in the polarization curves of cp Cu and the laser-fabricated specimens due to the oxidation of Cu to Cu^+. Compared with cp W, cp Cu is nobler and oxidized to Cu_2O/CuO in neutral solution in aerated oxidizing conditions. In neutral NaCl solution, oxygen participates in the corrosion reaction. However, the anodic reaction results in the formation of Cu_2O:

$$2Cu + H_2O \rightarrow Cu_2O + 2H^+ + 2e^- \qquad (5)$$

and subsequent oxidation of Cu_2O to CuO film at higher potentials according to:

$$Cu_2O + H_2O \rightarrow 2CuO + 2H^+ + 2e^- \quad (8)$$

The corrosion resistance of the laser-fabricated specimens with W (55 to 60 wt%) in 3.5 wt% NaCl solution decreased with the increase in Cu content and this finding is consistent with that of Levy and Chang who reported that the heavy W alloys with higher Cu content are more susceptible to chloride ion attack [25]. A local breakdown of the oxide layer of the Cu phase initiates corrosion attack owing to preferential adsorption of the chloride ions on the specimen surface, which subsequently hinders repassivation at local sites. Although the laser-fabricated specimens do not show considerable passivity as cp W and thermodynamic stability is not as noble as cp Cu, they have lower corrosion current densities than that of cp Cu (improved at most by a factor of 6.3). It is probably attributed to the presence of the passivable W phase in the NaCl solution.

3.2.2 In SAR

In SAR (pH 3.5), typical passivation behavior can be clearly observed in cp W. That is, when cp W is anodically polarized to a more positive potential, the corresponding anodic current density remains constant. In acidic media, passivation of W is due to the presence of tungsten oxides [35]. Below pH 5, W forms a passive anodic oxide film of WO_2 / W_2O_5 (at intermediate potentials) or WO_3 (at high potentials) [37]. W undergoes the following reactions:

$$W + 2H_2O \rightarrow WO_2 + 4H^+ + 4e^- \quad (6)$$

$$2WO_2 + H_2O \rightarrow W_2O_5 + 2H^+ + 2e^- \quad (7)$$

$$W_2O_5 + H_2O \rightarrow 2WO_3 + 2H^+ + 2e^- \quad (8)$$

Insoluble WO_3 passive film is formed and retards the dissolution of the W. Anik

reported that the increase in current density with potential for W results from the oxidation of a lower oxidation state W-oxide (WO_2) to a higher oxidation state W-oxide (W_2O_5 or WO_3) in acidic solutions. But the formation of a barrier layer (WO_3) and hydrated layer ($WO_3 \cdot xH_2O$) on the W surface does not allow the current density to increase further and it becomes potential independent [38].

For the laser-fabricated specimens in SAR, the passivity of W (cathode) enhances the dissolution of Cu binder (anode), which starts at the phase boundaries and propagates into the Cu phase according to the following anodic reaction:

$$Cu \rightarrow Cu^{2+} + 2e^- \quad (9)$$

In the SAR with the presence of air, dissolved O_2 promotes dissolution of Cu by providing the following cathodic reaction:

$$O_2 + 4H^+ + 4e^- \rightarrow 2H_2O \quad (10)$$

The large cathodic (W) area relative to the anodic (Cu) sites further accelerated the dissolution of Cu.

3.3 Evolution of corrosion by immersion tests

Generally, the corrosion behavior of alloys containing different metallic phases depends on their relative volume fractions, compositional distribution, reactivity [39-44] and the kinetics of the solid-state diffusion of the alloyed elements [45] leading to micro-galvanic coupling and hence preferential dissolution of the active phase. The evolution of corrosion of the laser-fabricated specimens with Cu and W phases was revealed by immersion tests.

3.3.1 In 3.5 wt% NaCl solution

For cp Cu immersed in 3.5 wt% NaCl solution (pH 7) for 1 week, corrosion

attack initiated at random locations as shown in Fig. 7(a). Longer exposure to the NaCl solution from 3 to 9 weeks resulted in more severe damage on the surface of cp Cu as shown in Fig. 7(b)-(d). On the other hand, cp W was slightly attacked at the grain boundaries after 9 weeks as shown in Fig. 8(b). At free corrosion potential, W corroded in the NaCl solution at a rate much slower (by 2 orders of magnitude) than that of cp Cu, as reflected by the lower I_{corr} (Table 2).

It could be observed from Figs. 9 and 10 that the surface of the laser-fabricated specimens (LA-W-Cu-p1.8 and LA-W-Cu-p2) in 3.5 wt% NaCl solution has undergone significant selective corrosion attack at the Cu phase. From the SEM micrographs of the laser-fabricated specimens immersed in 3.5 wt% NaCl solution for 1 week [Figs. 9(a) and 10(a)], corrosion attack started at the W-Cu phase boundaries and propagated into the Cu phase while the W particles remain intact. Gradual loss of the Cu phase and then complete detachment of W particles can be observed in later stages as shown in Fig. 9(b)-(d) and Fig. 10(b)-(d). From Figs. 9(d) and 10(d), the extensive corrosion of Cu phase led to detachment of the W particles, leaving behind holes on the surface.

It is interesting to note that in NaCl solution, Cu is cathodic to W, but the Cu phase in the laser-fabricated specimens dominantly dissolved in the immersion test, seemingly behaving as the anodic phase. An explanation on this apparently contradictory observation is proposed below. When the laser-fabricated specimens were immersed in the NaCl solution, their *OCP* values (-0.319 V_{SCE} and -0.337 V_{SCE} for LA-W-Cu-p1.8 and LA-W-Cu-p2 respectively) were lower than the *OCP* of cp Cu (-0.217 V_{SCE}) and higher than the *OCP* of cp W (-0.444 V_{SCE}). However, as all these *OCP* values were quite near to each other, both cathodic and anodic reactions took place on Cu and W phases in a non-negligible manner. In other words, the anodic and cathodic current densities were all not negligible for the Cu and W phases. The anodic

current densities corresponded to dissolution or corrosion, while the cathodic current densities corresponded to oxygen or water reduction. As the anodic current density of the Cu phase was greater than the anodic current density of the W phase, the Cu phase was corroding more quickly than the W phase even though the Cu phase was cathodic to the W phase. This anomalous observation is possible depending on the relative electrode kinetics around the *OCP*. So dominant dissolution of Cu binder occurred, and the Cu phase enclosing the W was gradually removed until it could not hold the W particles. The W particles were finally detached. When the topmost Cu binder was dissolved, the underlying Cu binder was exposed. Compared with the XRD patterns of the laser-fabricated specimens before immersion test (Fig. 4), the XRD patterns of the laser-fabricated specimens after immersion tests show significant decrease in intensity of W peaks due to W removal via particle detachment (Fig. 11).

3.3.2 In SAR

For cp Cu and cp W, the grain boundaries were revealed after immersion in SAR for 9 weeks as shown in Fig. 12 and Fig. 13 respectively. Corrosion attack was also observed at the porosities of cp W (Fig. 13), with the formation of WO_3 as the corrosion product.

On the other hand, the corrosion morphology for the laser-fabricated specimens corroded in SAR (pH 3.5) is different from that in 3.5 wt% NaCl solution (pH 7). For the laser-fabricated specimens, it is observed that corrosion took place initially at the boundaries of the Cu phases [Fig. 14(a) and Fig. 15(a)] while the W particles became fuzzy due to oxidation to WO_3 as depicted in Fig. 14(d) and Fig. 15(d). In SAR, the Cu phase acted sacrificially and the present finding differs from that of Ogundipe's group. They reported that the heavy W alloy with Cu (W-5.1wt%Cu) in 10^{-4} M HCl (pH 4) suffered from preferential corrosion at the W grains [26]. Such contradictory

results may be attributed to the higher W content in W-5.1wt%Cu as compared with the laser-fabricated specimens (55-60 wt%W). However, the Ni–Fe binder used in other heavy W alloys tested in 10^{-4} M HCl (pH 4) has been found to be more active than W. It is attributed to the solubility of W into this phase (in contrast, W has negligible miscibility in Cu-containing binder phases) and also due to the protective nature of the air-formed passive film on W [26].

In SAR (pH 3.5), W was stable at *OCP* and was passive. The phase boundaries of Cu phase (anode) were selectively attacked and dissolved, while the W particles (cathode) were still intact but passive as shown in Fig. 14(a) and Fig. 15(a). At the later stage, the W particles became detached, exposing the Cu phase left behind and leading to a large crater as shown in Figs. 14(d) and 15(d).

When selective dissolution of Cu binder occurred, the topmost layers of the laser-fabricated specimens were depleted in the noble phase (W). The XRD patterns of the laser-fabricated specimens after immersion test in SAR also show significant decrease in the intensity of W peaks (Fig. 16). Initially, W content was higher than Cu content in the laser-fabricated specimens, and preferential dissolution of Cu binder occurred, leading to massive loss in W particles.

4. Conclusions

(i) Laser fabrication of W-reinforced Cu layers has been successfully achieved using a HPDL resulting in W content of 55 and 60 wt% in the laser-modified zones. The microstructure of the laser-fabricated specimens consists of micron-sized W particles in a Cu matrix without porosity.

(ii) In both 3.5 wt% NaCl solution (pH 7) and SAR (pH 3.5), the *OCP* of the laser-fabricated specimens are more active as compared with cp Cu while their corrosion current densities are lower than that of cp Cu attributed to the presence

of the passivable W phase.

(iii) Although Cu is cathodic to W in 3.5 wt% NaCl solution, the Cu phase in the laser-fabricated specimens dominantly dissolves during the immersion test. As the *OCP* values of the laser-fabricated specimens, cp Cu and cp W are quite near to each other, the anodic and cathodic current densities are all not negligible for the Cu and W phases. As the anodic current density of the Cu phase is greater than anodic current density of the W phase, the Cu phase corrodes more quickly than the W phase. This anomalous observation is possible depending on the relative electrode kinetics around the *OCP*.

(iv) For the laser-fabricated specimens immersed in SAR, the Cu phase is anodic while the W phase is passive due to the formation of WO_3. Cu phase is selectively attacked and W particles are finally detached from the Cu binder leading to large craters.

Acknowledgements

The work described in this manuscript was fully supported by research grants from the Science and Technology Development Fund (FDCT) of Macau SAR (Grant no. FDCT 070/2011/A3).

References

[1] F. Habashi (Ed), Alloys Preparation, Properties, Applications, Wiley-VCH Weinheim, (1998), p. 245.

[2] X. L. Peng, Preparation of nickel and copper coated fine tungsten powder, Mater. Sci. Eng. A262 (1999) 1.

[3] T. Raghu, R. Sundaresan, P. Ramakrishnan, Synthesis of nanocrystalline copper–tungsten alloys by mechanical alloying, Mater. Sci. Eng. A304–306

(2001) 438.

[4] V. Gauthier, F. Robaut and A. Upadhyaya, Effect of Fe on the constitution of Cu–W alloys at 1200 °C, J. Alloys Compd. 361 (2003) 222.

[5] S. Kac, J. Kusiński, SEM and TEM microstructural investigation of high-speed tool steel after laser melting, Mater. Chem. Phys. 81 (2003) 510.

[6] K. Zheng, S. Zhang, Study on laser carburizing and laser boron-carburizing of the #20 steel surface, Mater. Chem. Phys. 26 (1990) 57.

[7] Z.S. Yu, Z.K. Quan, The C-N-B laser alloying of the #5 steel surface, Mater. Chem. Phys. 25 (1990) 277.

[8] A. Hirose, K.F. Kobayashi, Surface alloying of copper with chromium by CO_2 laser, Mater. Sci. Eng. A174 (1994) 199.

[9] J. Dutta Majumdar, I. Manna, Laser surface alloying of copper with chromium II. Improvement in mechanical properties, Mater. Sci. Eng. A268 (1999) 227.

[10] S. Song, Z. Tang, The electrochemical behaviour of 2Cr13 steel treated by laser surface remelting, Mater. Chem. Phys. 28 (1991) 281.

[11] C.C. Huang, W.T. Tsai, J.T. Lee, Effects of N and Mo on the electrochemical behavior of laser-alloyed stainless steels in a 3.5 wt.% NaCl solution, Mater. Chem. Phys. 42 (1995) 280.

[12] P.H. Chong, Z. Liu, P. Skeldon, G.E. Thompson, Large area laser surface treatment of aluminium alloys for pitting corrosion protection, Appl. Surf. Sci., 208–209 (2003) 399.

[13] P.K. Wong, C.T. Kwok, H.C. Man, F.T. Cheng, Corros. Sci. 57 (2012) 228.

[14] S.H. Zhang, J.H. Yoon, M.X. Li, T.Y. Cho, Y.K. Joo, J.Y. Cho, Mater. Chem. Phys. 119 (2010) 458.

[15] J. Li, C. Chen, Q. He, Mater. Chem. Phys, 133 (2012) 741.

[16] X.B. Liu, H.Q. Liu, X.J. Meng, C.F. Sun, M.D. Wang, L.H. Qi, G.L. Shi, S.H.

Wu, Mater. Chem. Phys. 143 (2014) 616.

[17] H.R. Geng, Y. Liu, C.Z. Chen, M.H. Sun, Y.Q. Ga, Materials Science and Technology, 16 (2000) 564.

[18] Y. Sato, M. Hara, K. Masuda, Mater. Chem. Phys. 54 (1998) 186.

[19] M. Pons, M. Caillet, A. Galerie, Mater. Chem. Phys. 16 (1987) 423.

[20] L.W. Tsay, M.C. Young, F.Y. Chou, R.K. Shiue, Mater. Chem. Phys. 88 (2004) 348.

[21] J. Dutta Majumdar, I. Manna, Mater. Sci. Eng. A268 (1999) 216.

[22] R. Li, Y. Shi, J. Liu, Z. Xie, Z. Wang, Int J Adv Manuf Technol. 48 (2010) 597.

[23] D. Gu, Y. Shen, X. Wu, Materials Letters, 62 (2008) 1765.

[24] S.H. Wang, L. Xue, Laser cladding of W-Cu composite on bronze substrate Wang, Surface Engineering in Materials Science III, 2005 TMS Annual Meeting, February 13-17, San Francisco California, (2005) 2010-03.

[25] M. Levy, F. Chang, Corrosion behavior of high density tungsten alloys, Environmental Degradation of Engineering in Aggressive Environments, Proceedings of 2nd International Conference on Environmental Degradation of Engineering Materials, Blacksburg, Va, USAP. (1981) p. 33.

[26] A. Ogundipe, B. Greenberg, W. Braida, C. Christodoulatos, D. Dermatas, Corros. Sci. 48 (2006) 3281.

[27] P.K. Wong, C.T. Kwok, H.C. Man, D. Guo, Laser fabrication of W reinforced Cu layers: II. Electrical erosion behavior in air and synthetic acid rain, submitted to Mater. Chem. Phys.

[28] G. Dehm, B. Medres, L. Shepeleva, C. Scheu, M. Bamberger, B.L. Mordike, S. Mordike, G. Ryk, G. Halperin, I. Etsion, Wear 225–229 (1999) 18.

[29] R. Jendrzejewski, G. Sliwinski, Investigation of temperature and stress fields in laser cladded coating, Appl. Surf. Sci. 254 (2007) 921–925.

[30] Standard Reference Test Method for Making Potentiodynamic Anodic Polarization Measurements, ASTM G5-94, annual Book of ASTM Standards, Vol. 03.02, ASTM, Philadelphia, 1995.

[31] Annual air quality report, Macao Meteorological and Geophysical Bureau, Macao Special Administration Region, 2010.

[32] W. M. Steen, J. Mazumder, Laser Material Processing, 4th ed., Springer (2010) p.90.

[33] L. Dubourg, H. Pelletier, D. Vaissiere, F. Hlawka, A. Cornet, Wear 253 (2002) 1077.

[34] Army Missile Command Report RS-TR-67-11, "Practical Galvanic Series", 1997. (http://www.corrosion-doctors.org/Definitions/galvanic-series.htm)

[35] M. Pourbaix, Atlas of Electrochemical Equilibria in Aqueous Solutions, 2nd ed., NACE, Houston, 1974.

[36] R.S. Lillard, G.S. Kanner, D.P. Butt, J. Electrochem. Soc., 145 (1998) 2718.

[37] S. B. Lyon, Corrosion of tungsten and its alloys, Sherir Corrosion, Elsevier (2012) 2151.

[38] M. Anik, Electrochimica Acta 54 (2009) 3943.

[39] J.C. Lin, J.Y. Lin, S.P. Jou, Hydrometallurgy 43 (1996) 47.

[40] A. El Warraky, H.A. El Shayeb, E.M. Sherif, Anti-Corros Method M. 51 (2004) 52.

[41] J. R. Scully, T. O. Knight, R. G. Buchheit, D. E. Peebles, Corros. Sci. 35 (1993) 185.

[42] R. Ambat, N.N. Aung, W. Zhou, Corros. Sci. 42 (2000) 1433.

[43] N.N. Aung, W. Zhou, J. Appl. Electrochem. 32 (2002) 1397.

[44] N.N. Aung, W. Zhou, Corros. Sci. 52 (2010) 589.

[45] B.G. Ateya, H.W. Pickering, Corros. Sci. 38 (1996) 1245.

Table

Specimen	Thickness of laser-fabricated layer D (mm)	Dilution ratio (DR, %)	Cu content (wt%)	W content (wt%)
LA-W-Cu-p1.8	0.41	65	45	55
LA-W-Cu-p2	0.43	69	40	60

Table 1. Thickness, dilution ratio, compositions of laser-fabricated specimens.

	OCP in NaCl (V_{SCE})	I_{corr} in NaCl ($\mu A/cm^2$)	*OCP* in SAR (V_{SCE})	I_{corr} in SAR ($\mu A/cm^2$)
cp Cu	-0.217	8.974	-0.055	1.570
LA-W-Cu-p1.8	-0.319	1.312	-0.069	1.439
LA-W-Cu-p2	-0.337	1.096	-0.143	0.925
cp W	-0.444	0.926	-0.237	0.734

Table 2. Corrosion parameters of laser-fabricated specimens, cp Cu and cp W in 3.5 wt% NaCl solution and synthetic acid rain (SAR).

Legends of Tables

Table 1 Thickness, dilution ratio, hardness and W content of laser-fabricated specimens.

Table 2 Corrosion parameters of laser-fabricated specimens, cp Cu and cp W in 3.5 wt% NaCl solution and synthetic acid rain (SAR).

Figure

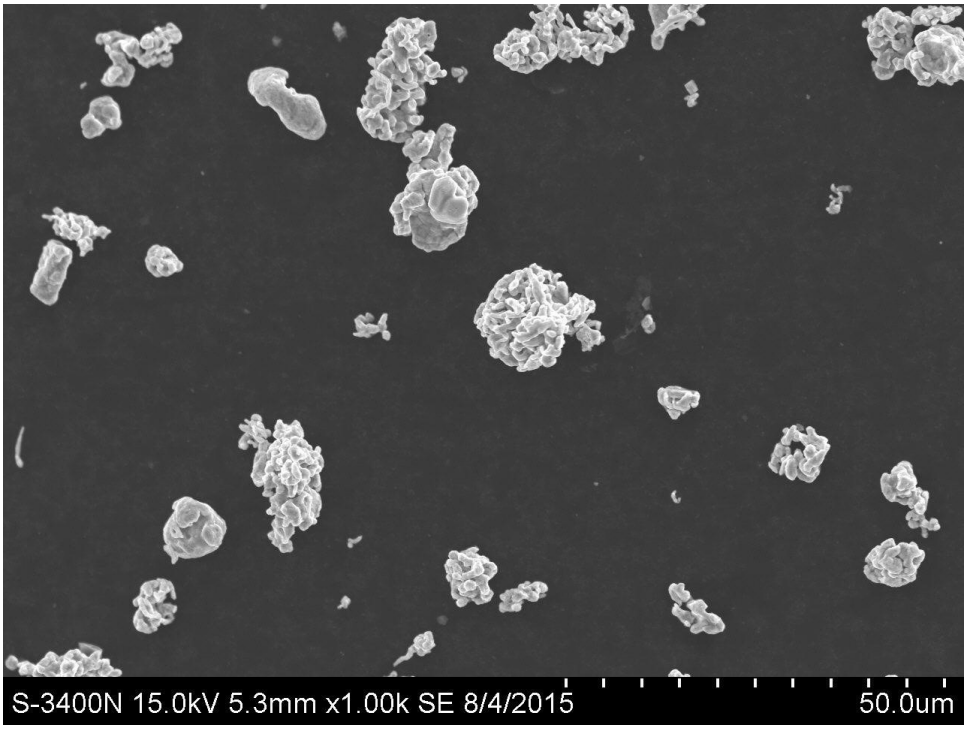

(a)

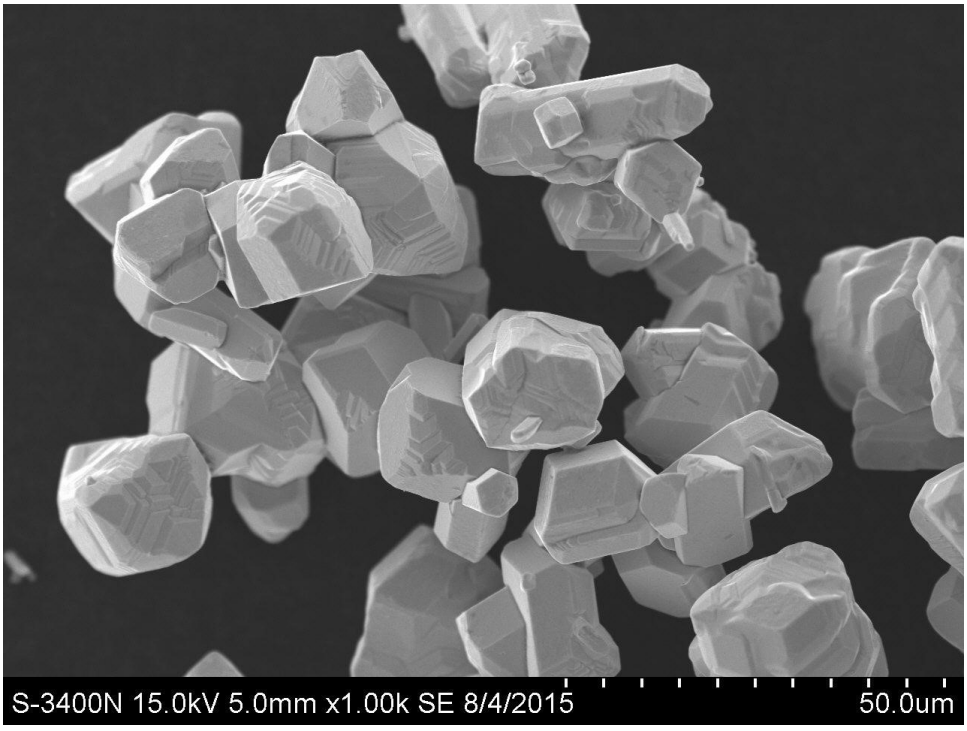

(b)

Fig. 1. SEM micrographs of morphology of (a) Cu and (b) W powders.

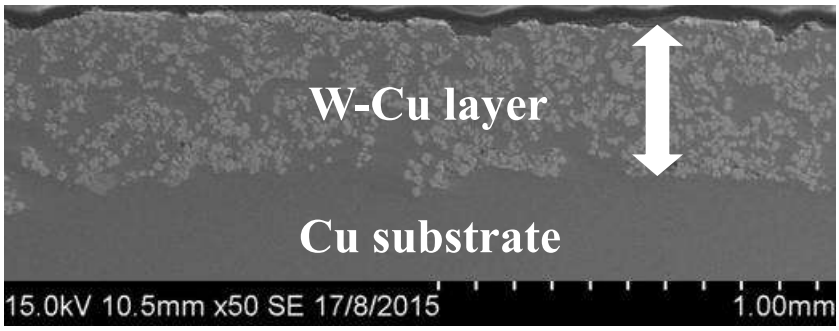

(a)

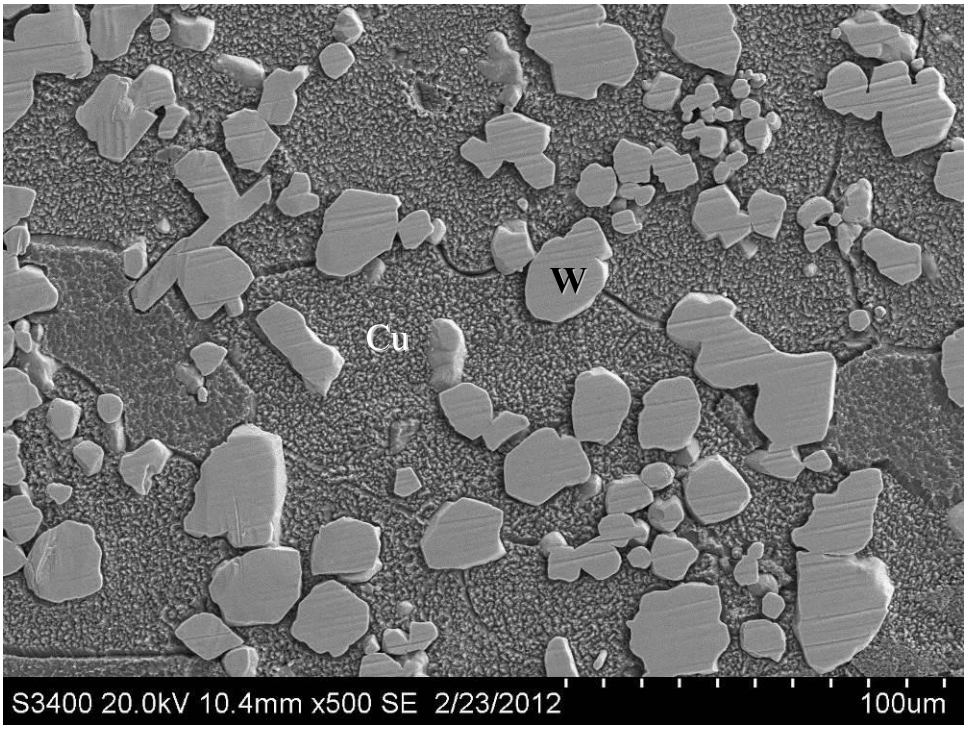

(b)

Fig. 2. Laser-fabricated specimen LA-W-Cu-p1.8 showing (a) cross-sectional view; and (b) Cu matrix embedded with W particles.

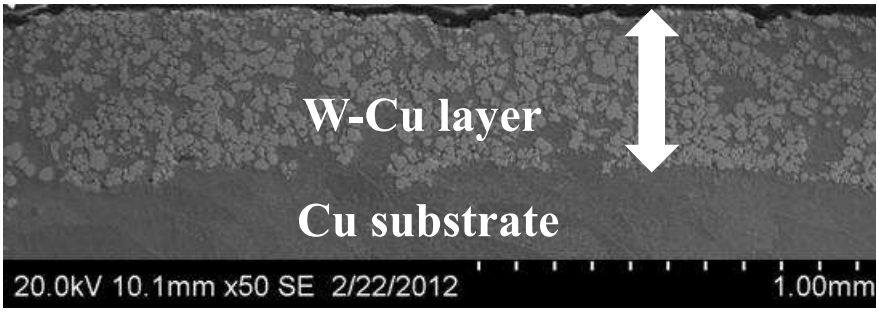

(a)

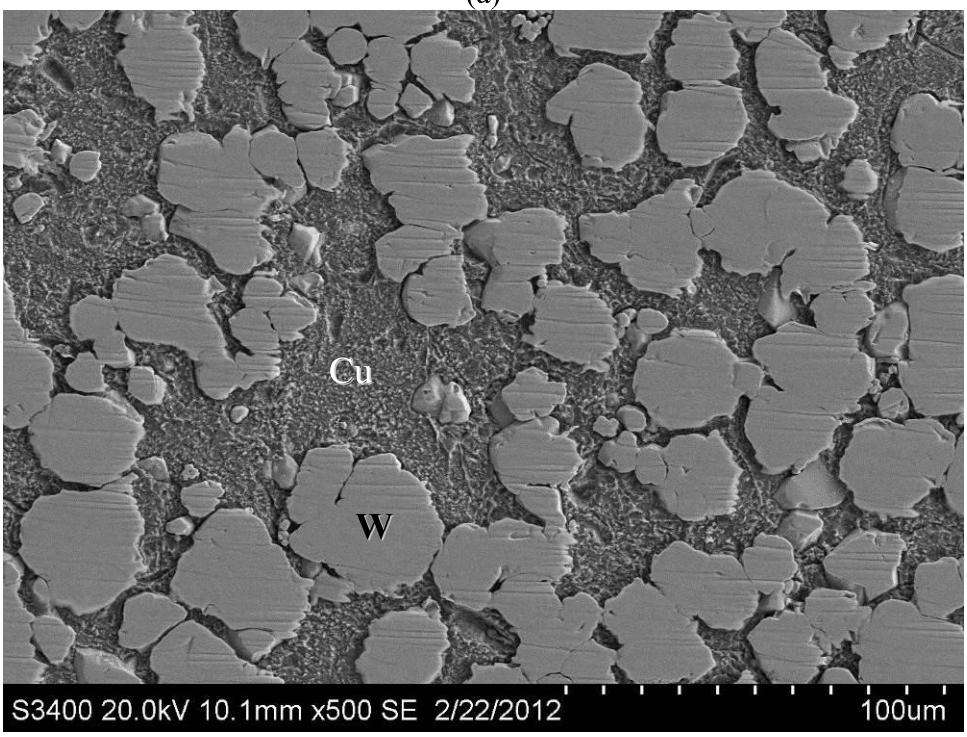

(b)

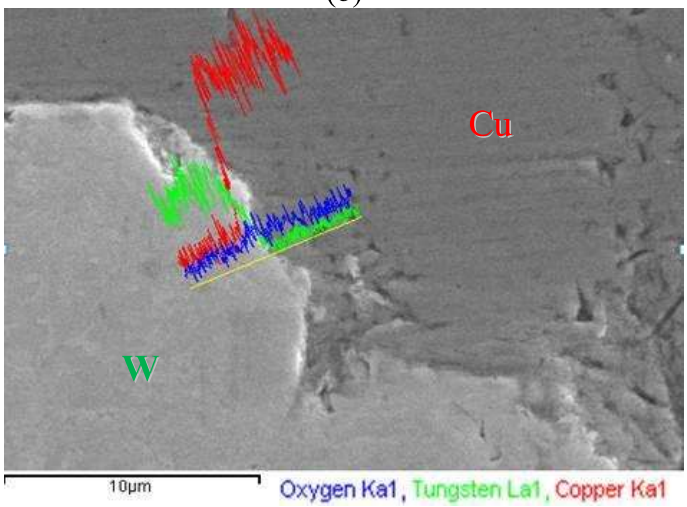

(c)

Fig. 3. Laser-fabricated specimen LA-W-Cu-p2 showing (a) cross-sectional view; (b) Cu matrix embedded with W particles; and (c) EDX line scan across the W and Cu phases.

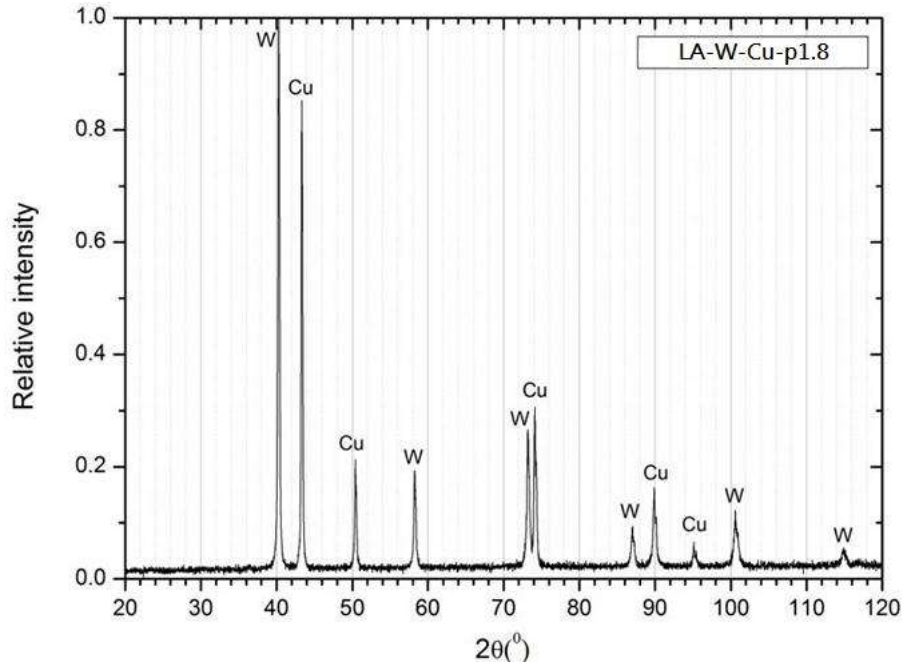

(a)

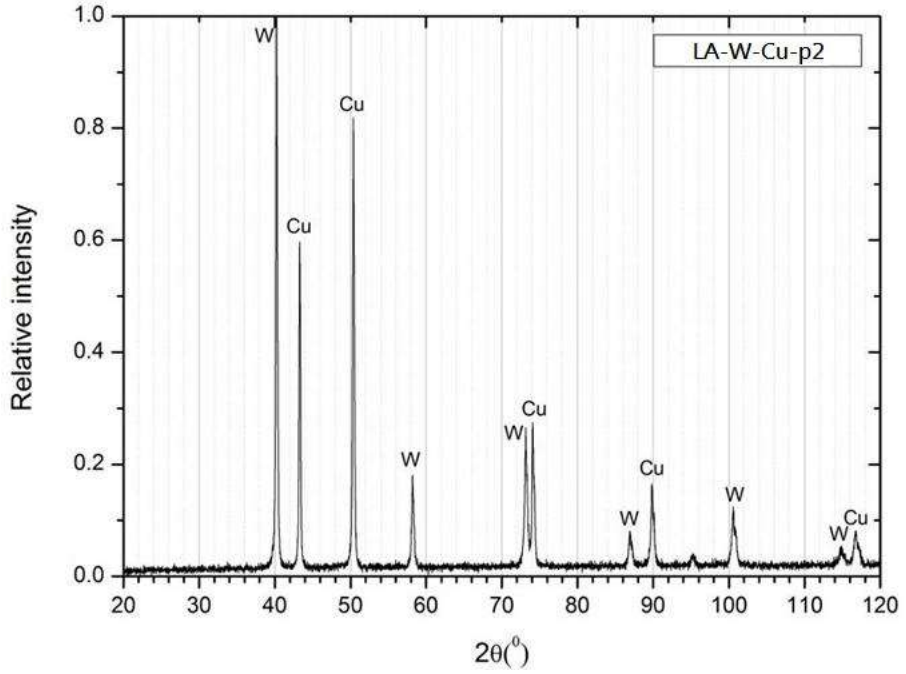

(b)

Fig. 4. XRD pattens of (a) LA-W-Cu-p1.8 and (b) LA-W-Cu-p2.

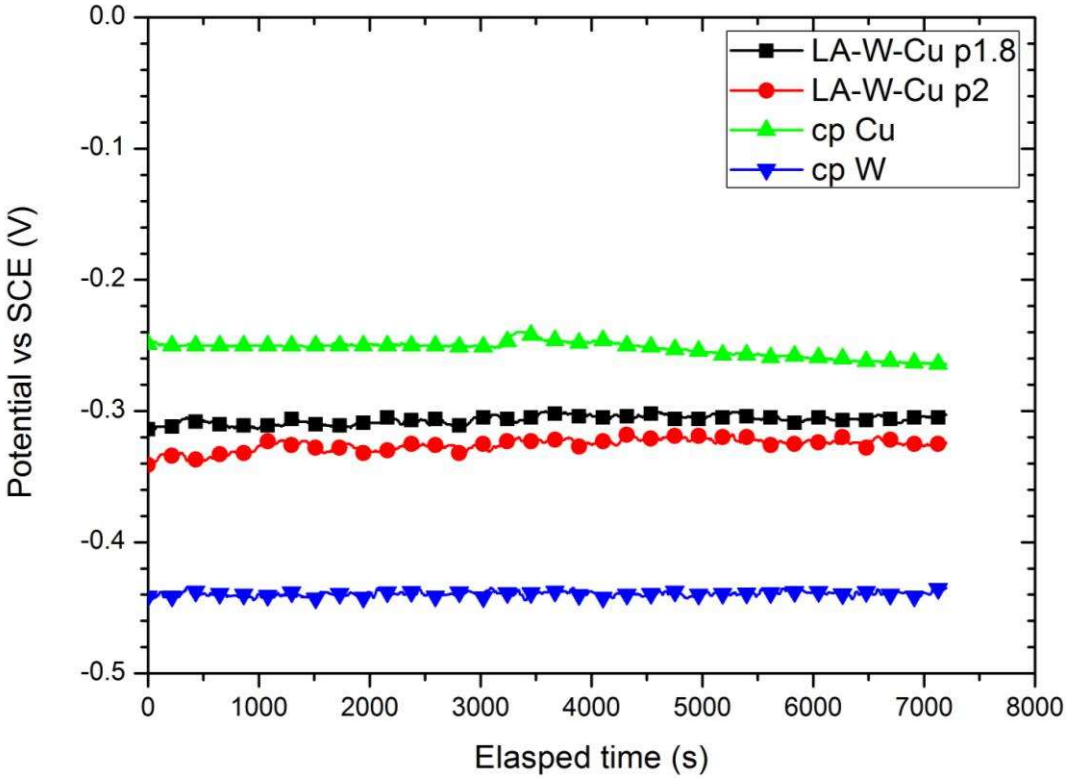

(a)

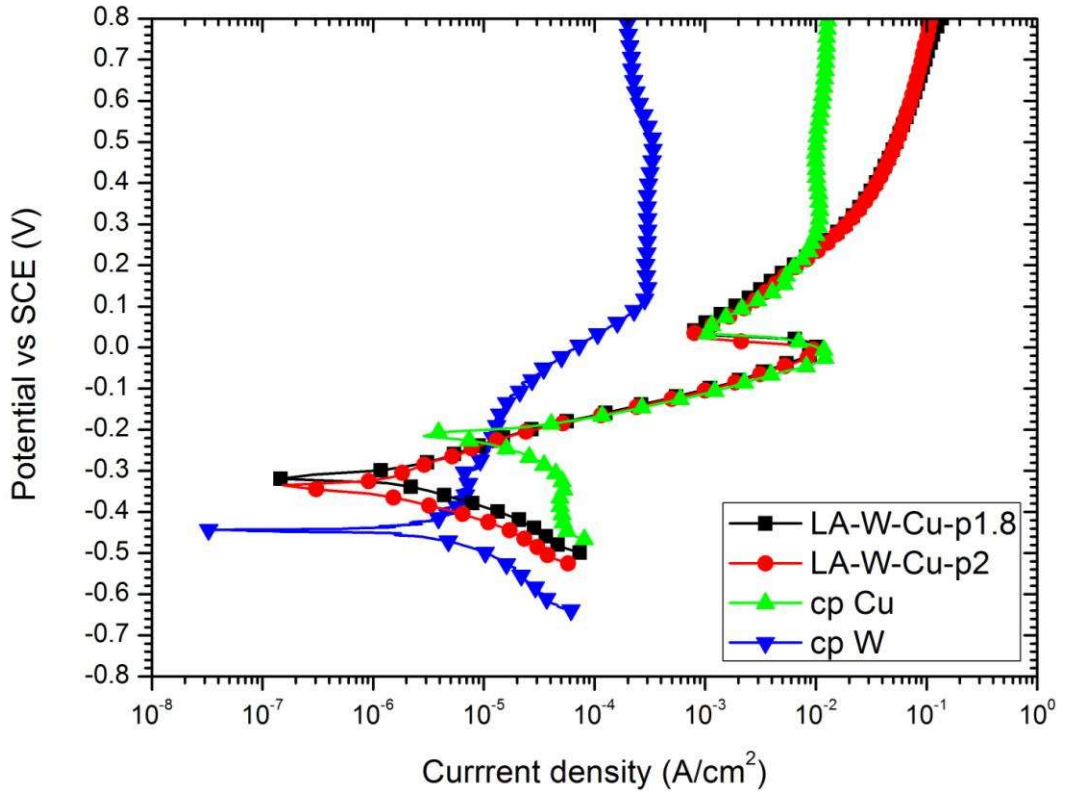

(b)

Fig. 5(a) Plot of OCP vs time and (b) potentiodynamic polarization curves of the laser-fabricated specimens, cp Cu and cp W in 3.5% wt% NaCl solution at 25 ^{o}C.

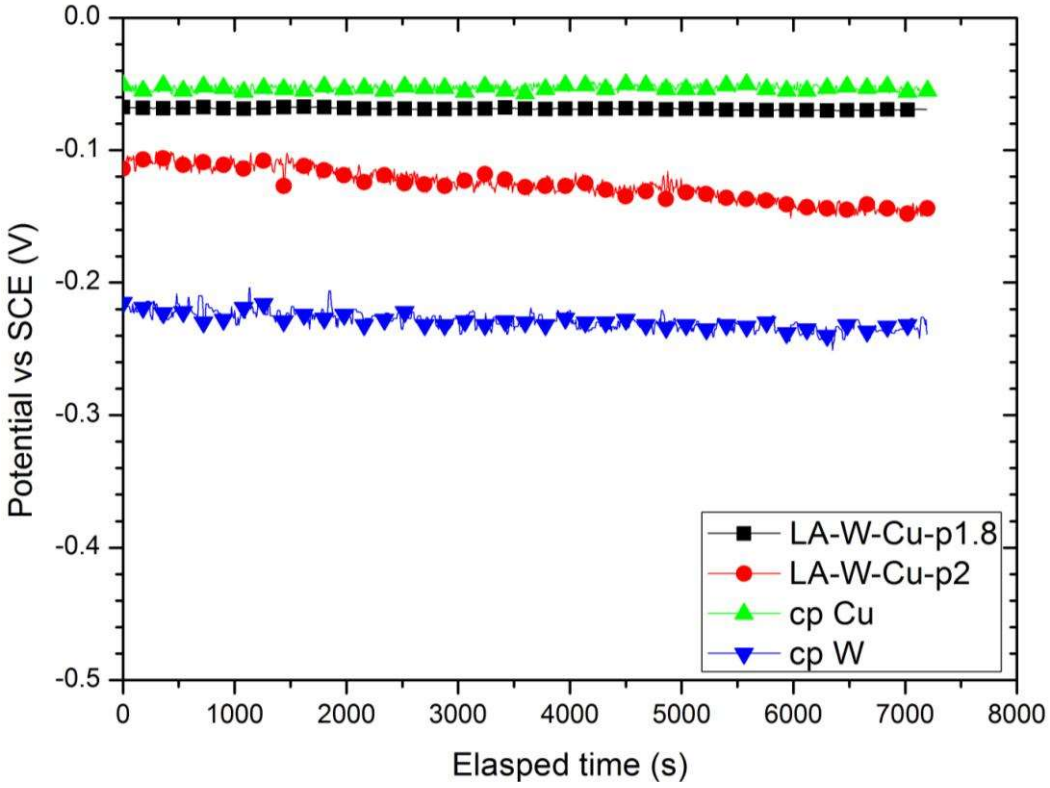

(a)

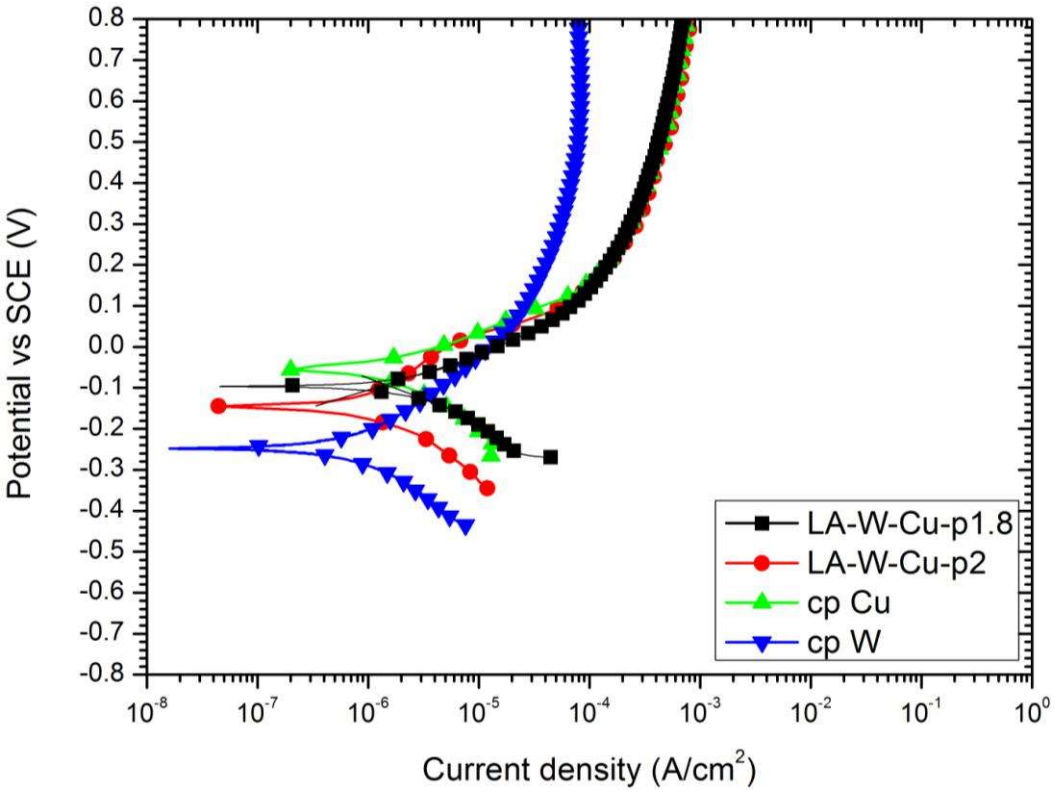

(b)

Fig. 6(a) Plot of OCP vs time and (b) potentiodynamic polarization curves of the laser-fabricated specimens, cp Cu and cp W in synthetic acid rain (SAR) at 25 ^{o}C

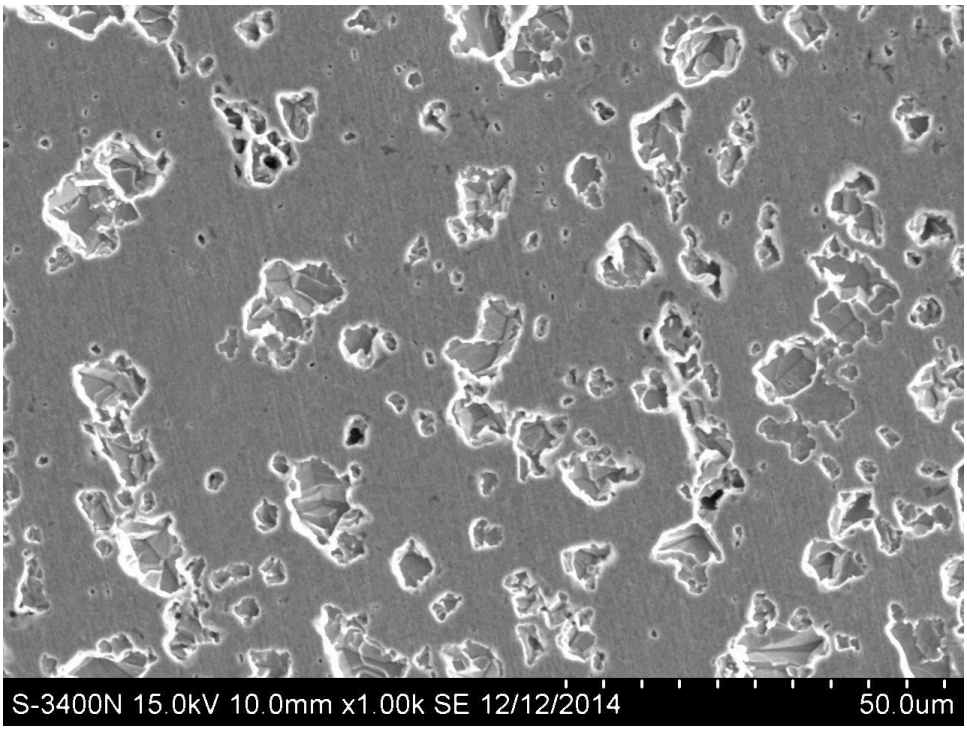
S-3400N 15.0kV 10.0mm x1.00k SE 12/12/2014
50.0um

(a)

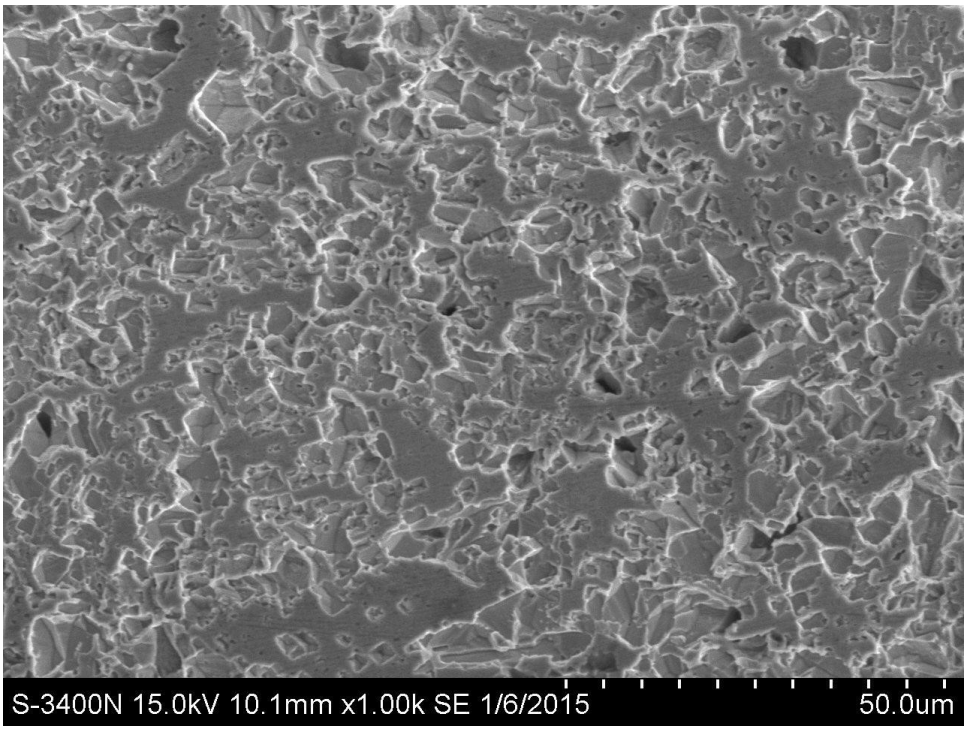
S-3400N 15.0kV 10.1mm x1.00k SE 1/6/2015
50.0um

(b)

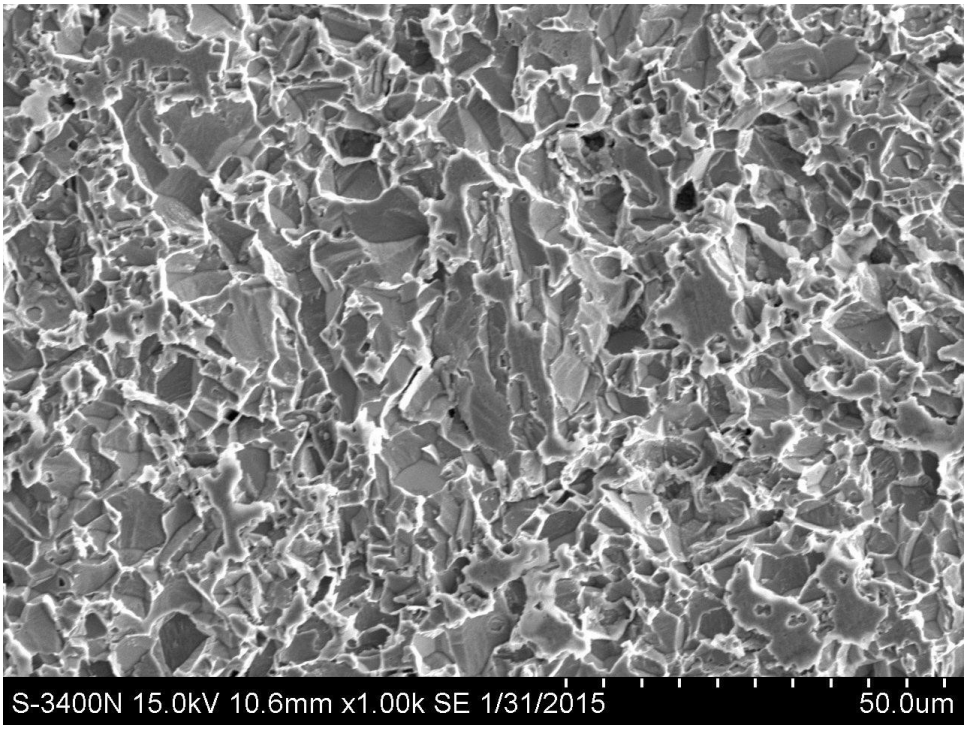

(c)

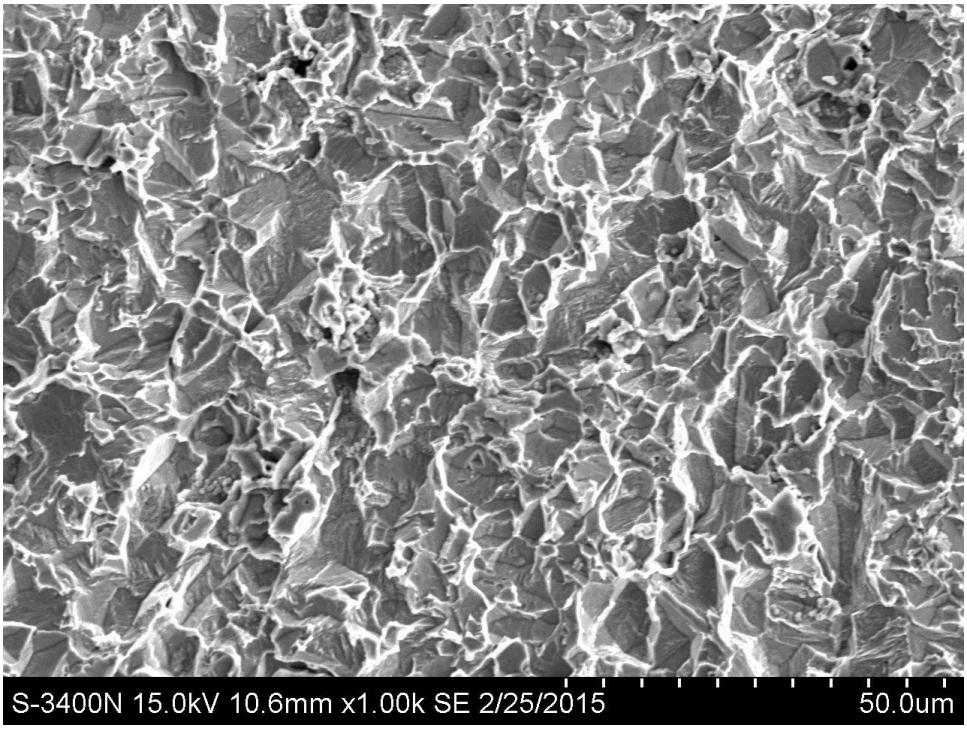

(d)

Fig. 7. Morphologies of corroded surface of cp Cu after immersion test in 3.5 wt% NaCl solution for different time: (a) 1 week; (b) 3 weeks; (c) 6 weeks; and (d) 9 weeks.

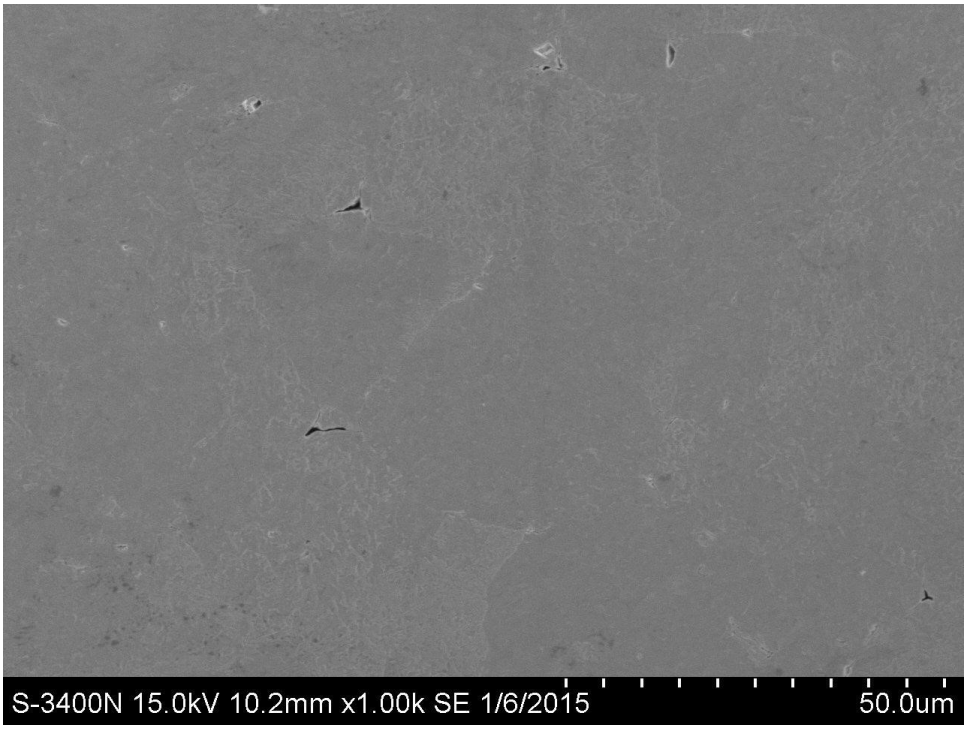

(a)

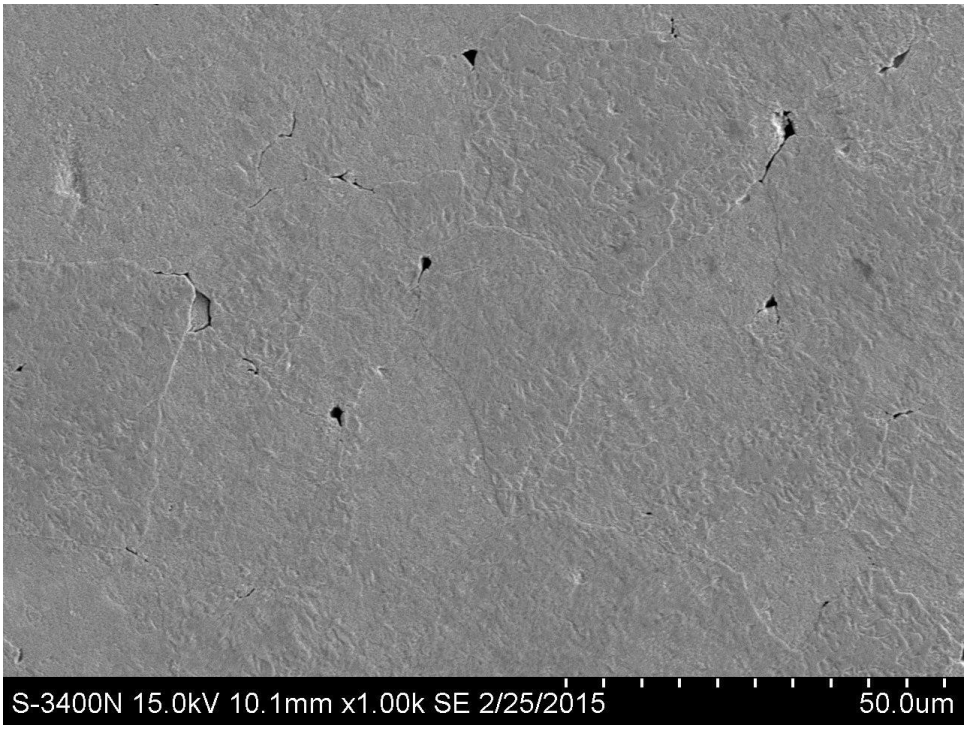

(b)

Fig. 8. Morphologies of corroded surface of cp W after immersion test in 3.5 wt% NaCl solution for different time: (a) 3 weeks; and (b) 9 weeks.

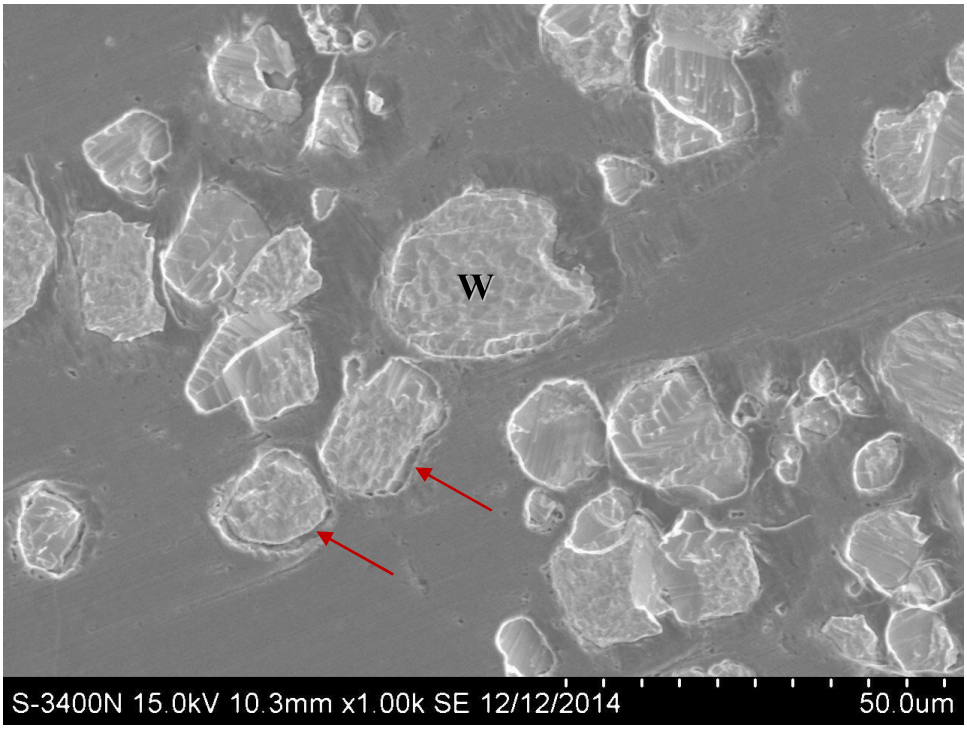
W
S-3400N 15.0kV 10.3mm x1.00k SE 12/12/2014
50.0um

(a)

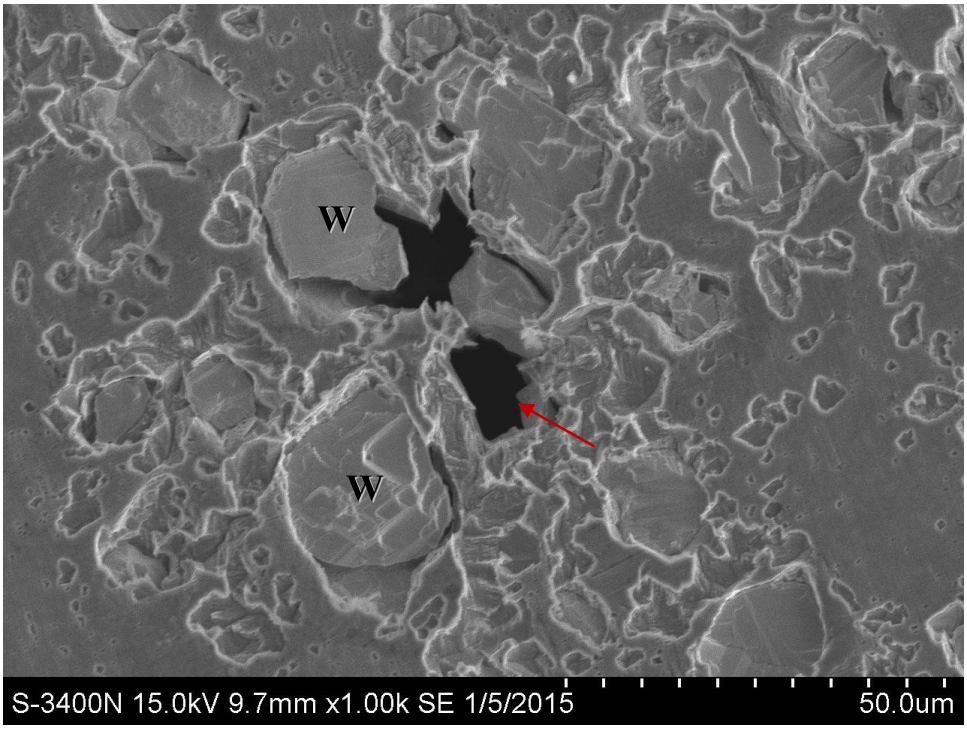
W
W
S-3400N 15.0kV 9.7mm x1.00k SE 1/5/2015
50.0um

(b)

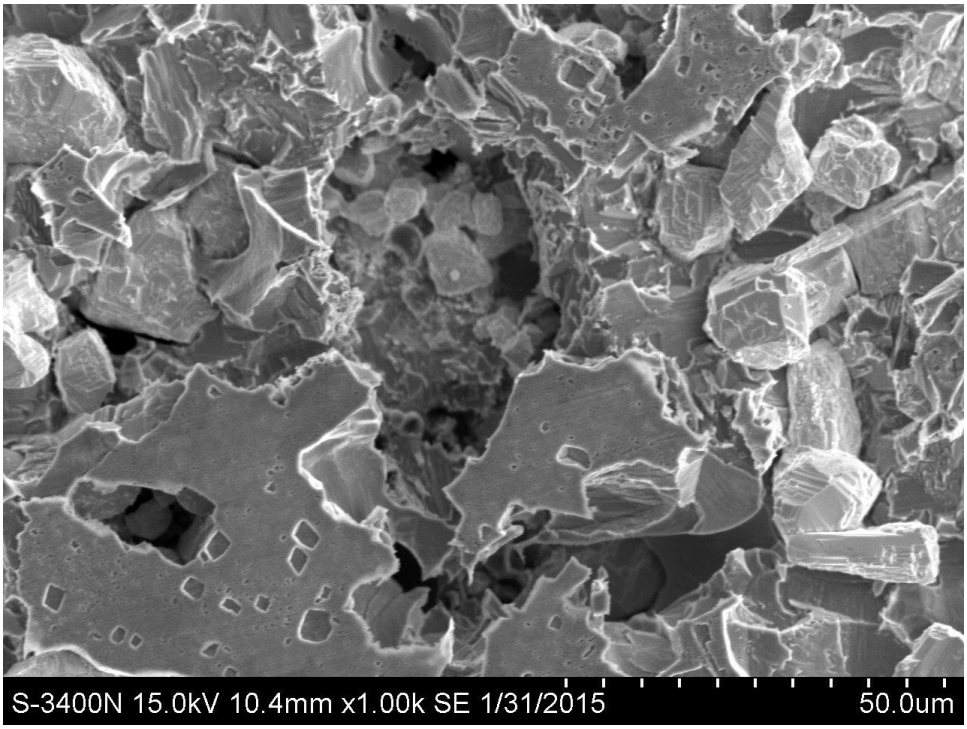

(c)

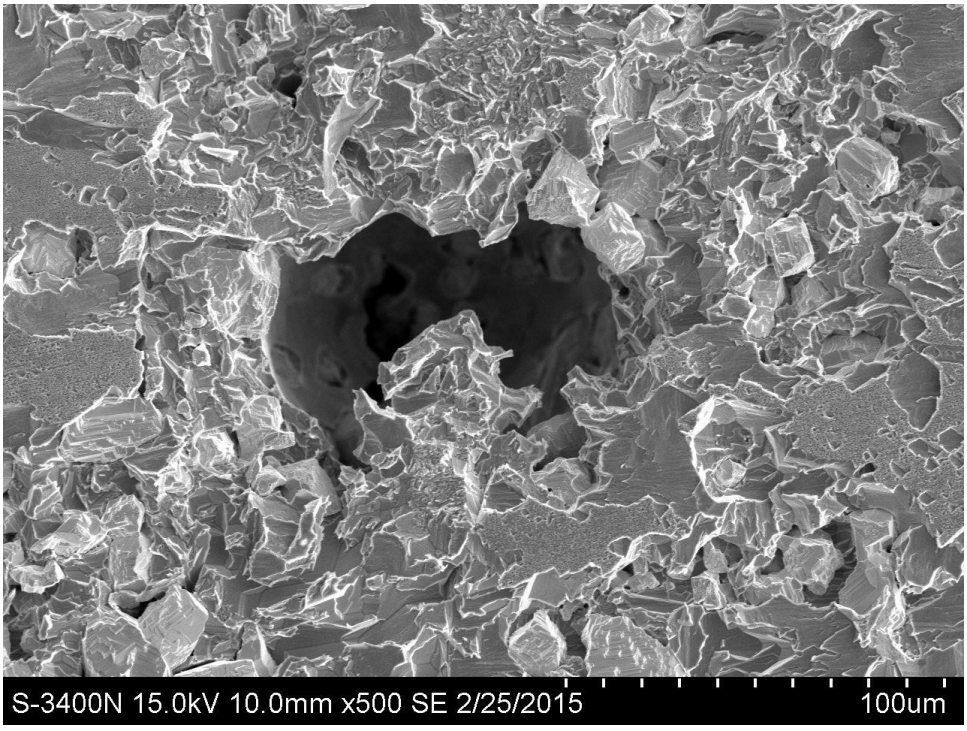

(d)

Fig. 9. Morphologies of corroded surface of LA-W-Cu-p1.8 after immersion test in 3.5 wt% NaCl solution for different time: (a) 1 week; (b) 3 weeks; (c) 6 weeks; and (d) 9 weeks.

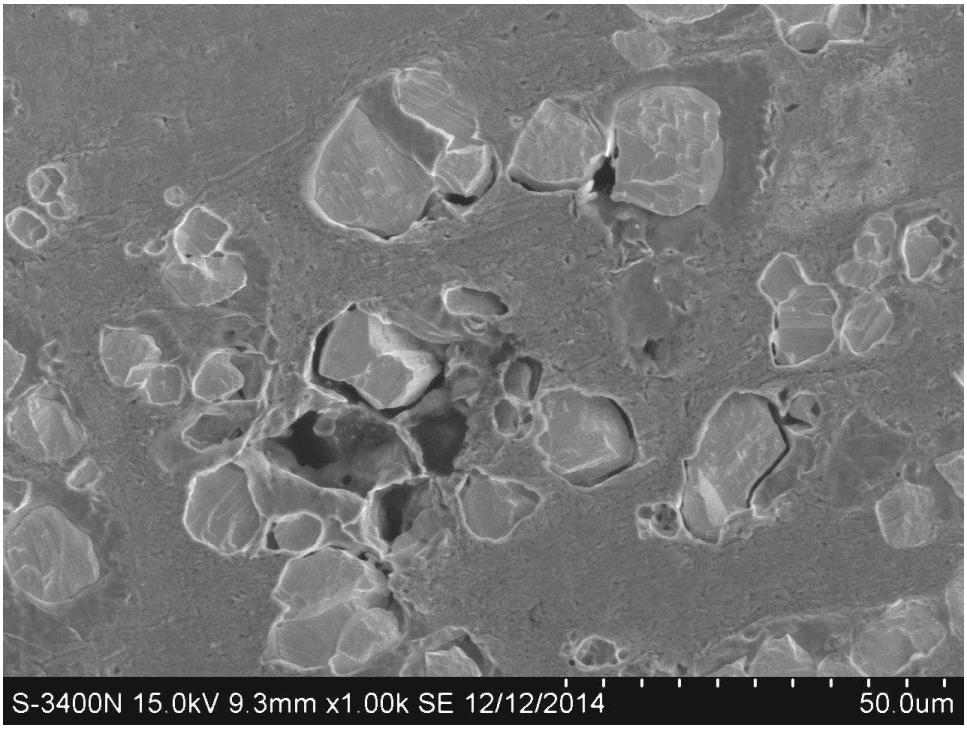
S-3400N 15.0kV 9.3mm x1.00k SE 12/12/2014
50.0um

(a)

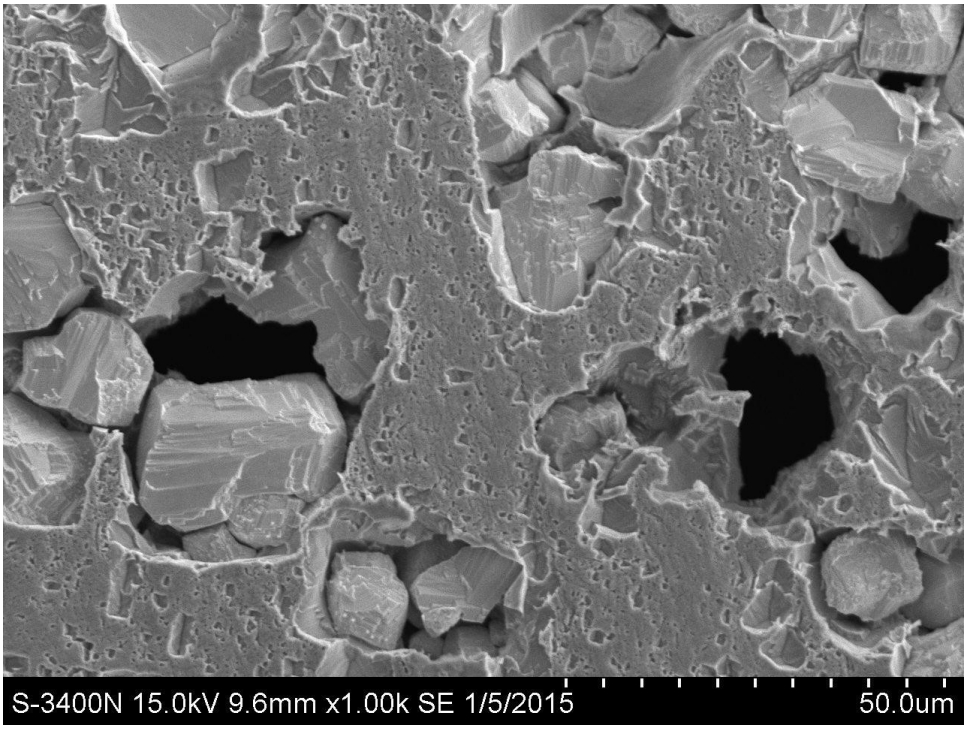
S-3400N 15.0kV 9.6mm x1.00k SE 1/5/2015
50.0um

(b)

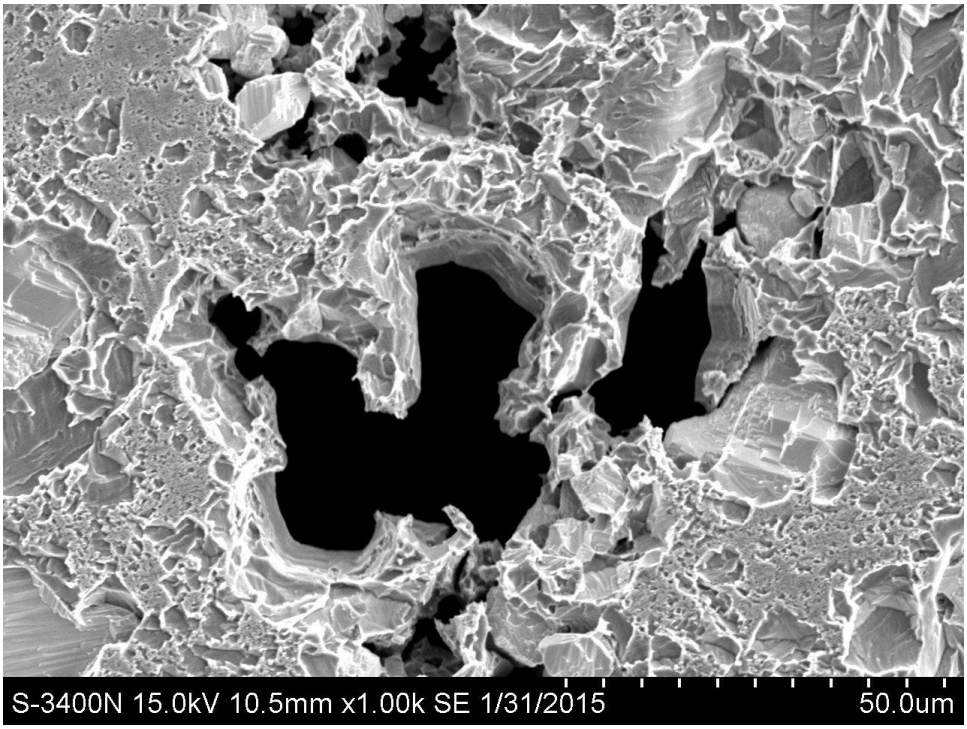

(c)

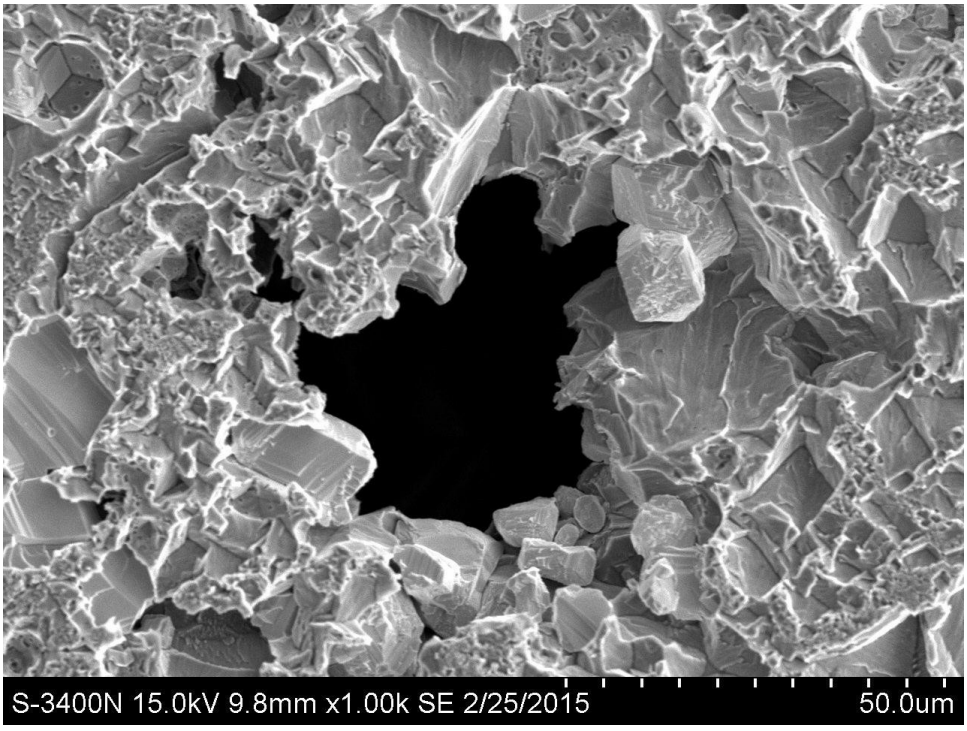

(d)

Fig. 10. Morphologies of corroded surface of LA-W-Cu-p2 after immersion test in 3.5 wt% NaCl solution for different time: (a) 1 week; (b) 3 weeks; (c) 6 weeks; and (d) 9 weeks.

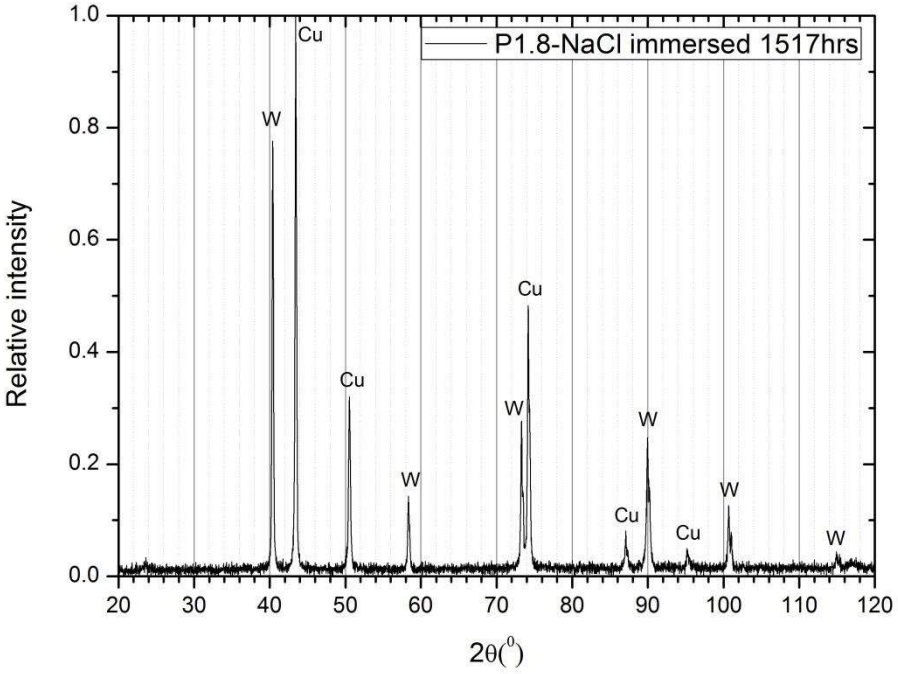

(a)

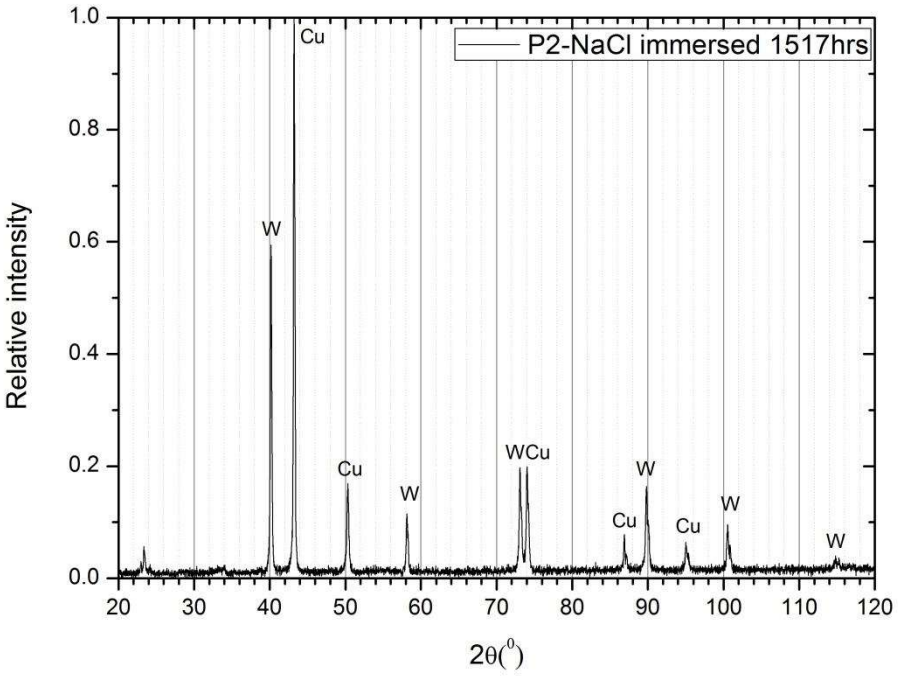

(b)

Fig. 11. XRD patterns of corroded surface of (a) LA-W-Cu-p1.8 and (b) LA-W-Cu-p2 in 3.5 wt% NaCl solution.

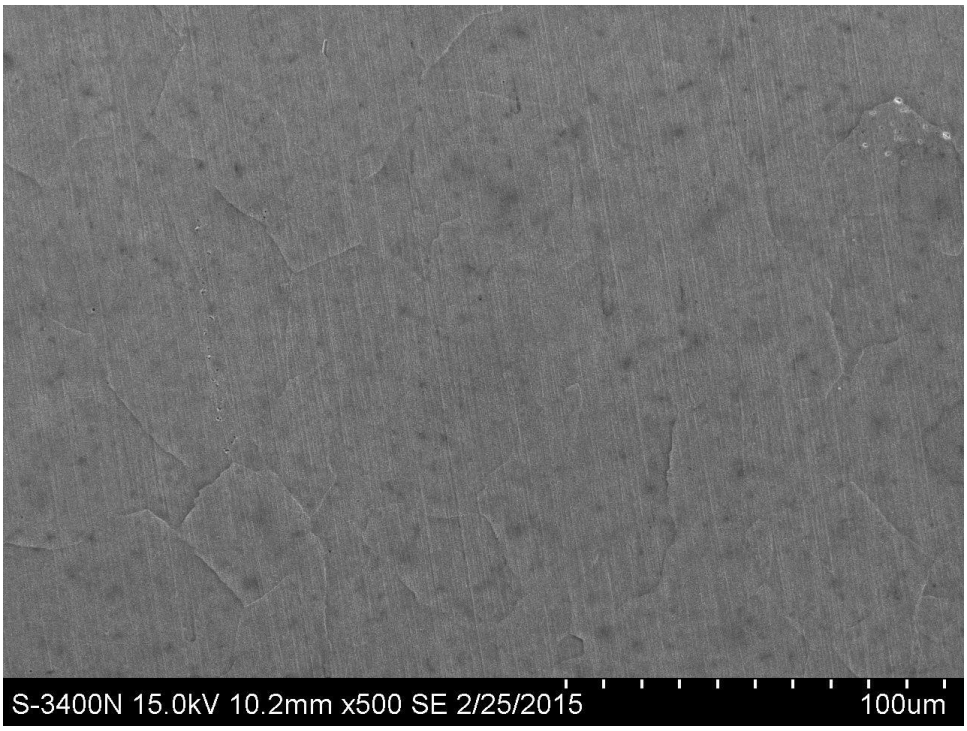

Fig. 12. Morphologies of corroded surface of cp Cu after immersion test in SAR for 9 weeks.

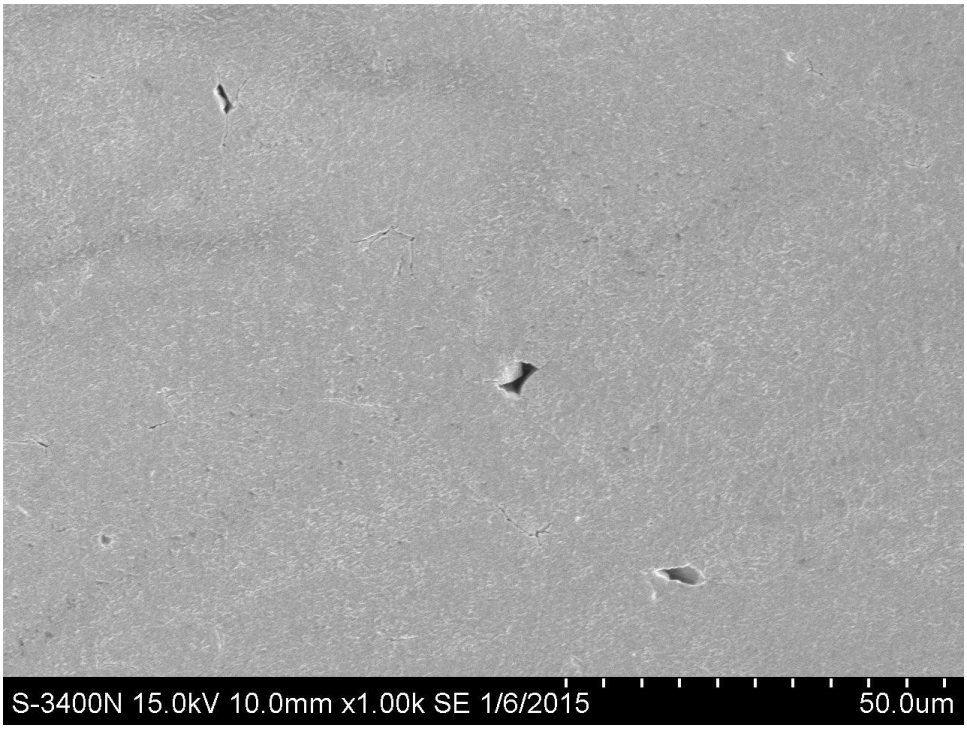

(a)

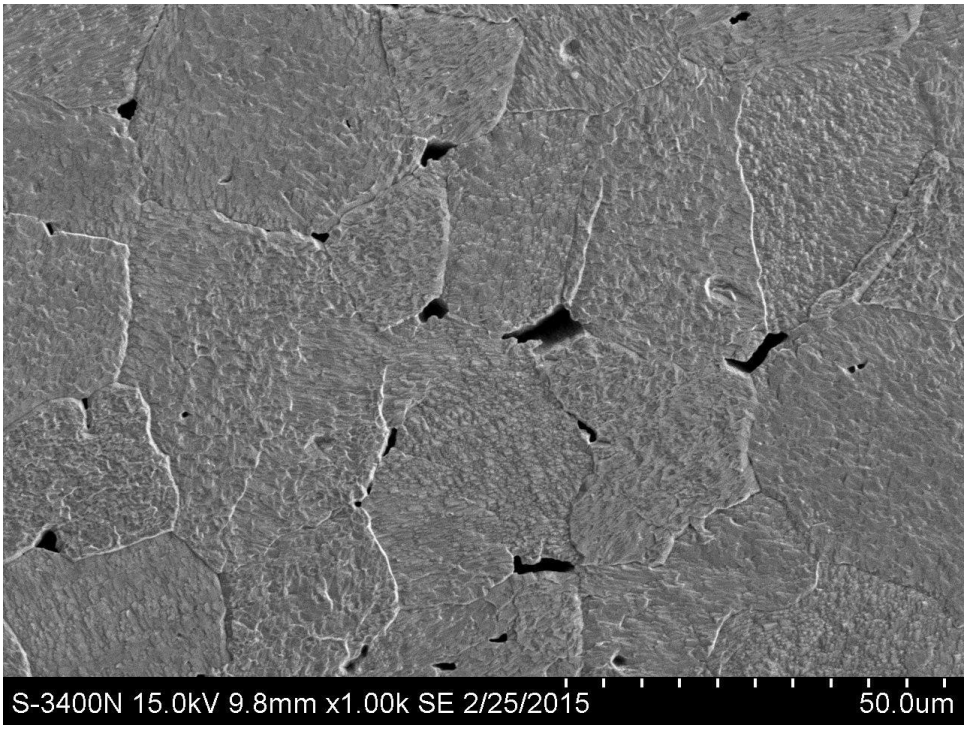

(b)

Fig. 13. Morphologies of corroded surface of cp W after immersion test in SAR for different time: (a) 3 weeks; and (b) 9 weeks.

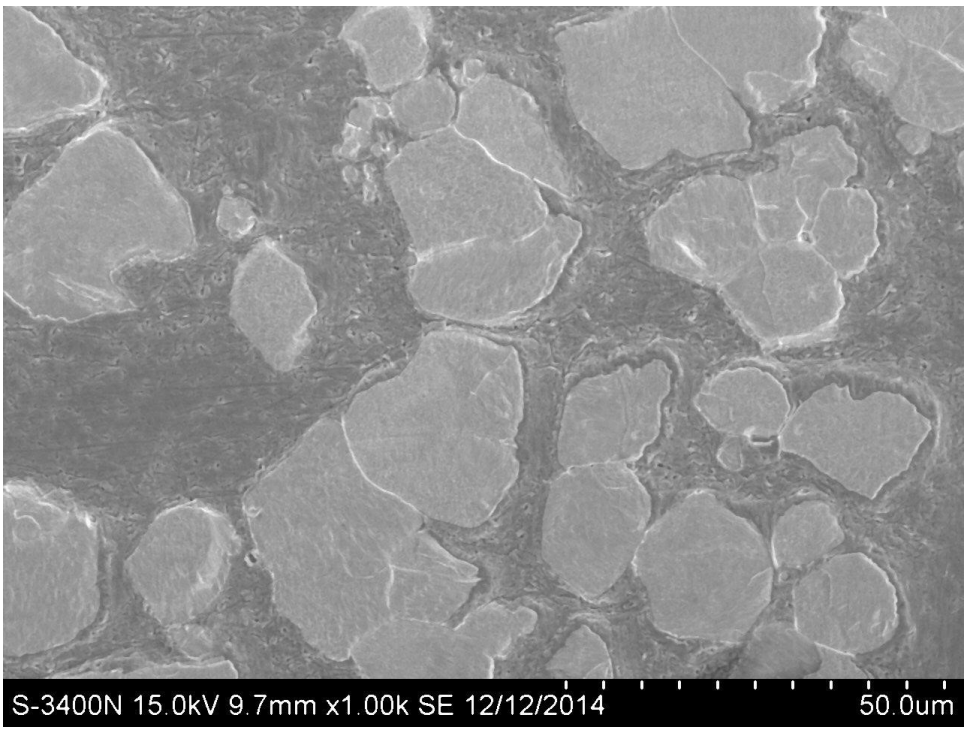
S-3400N 15.0kV 9.7mm x1.00k SE 12/12/2014
50.0um

(a)

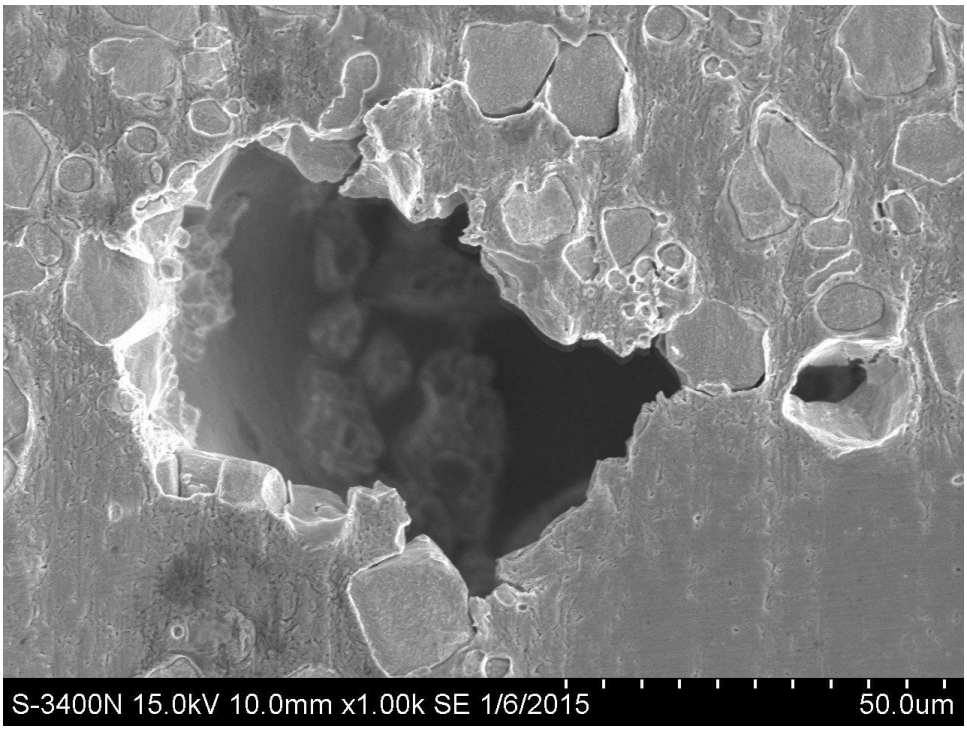
S-3400N 15.0kV 10.0mm x1.00k SE 1/6/2015
50.0um

(b)

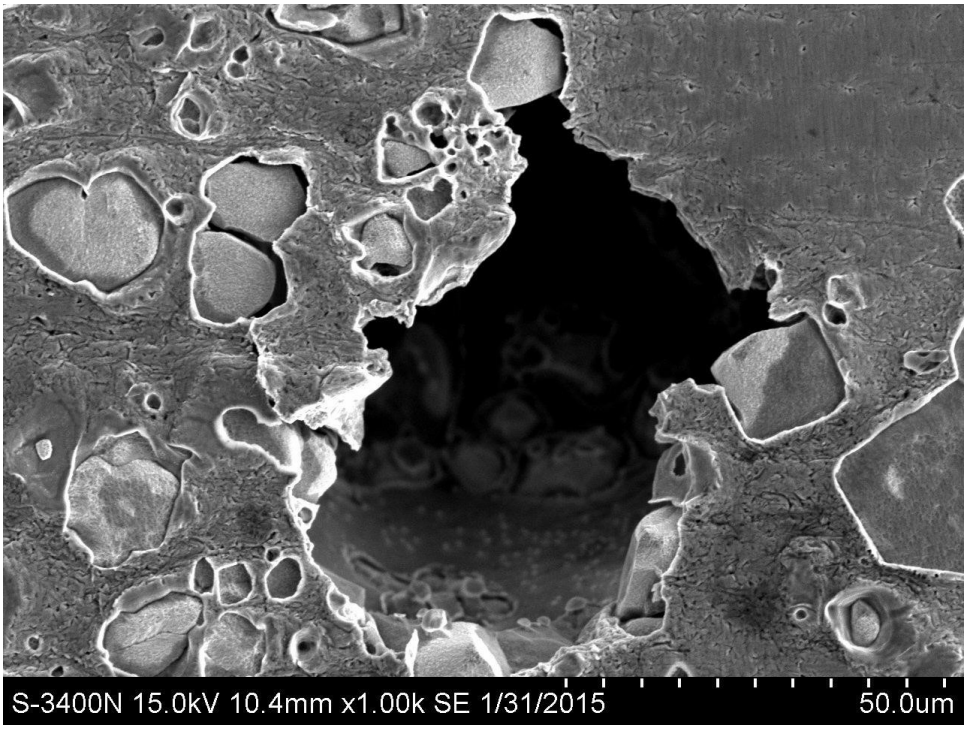

(c)

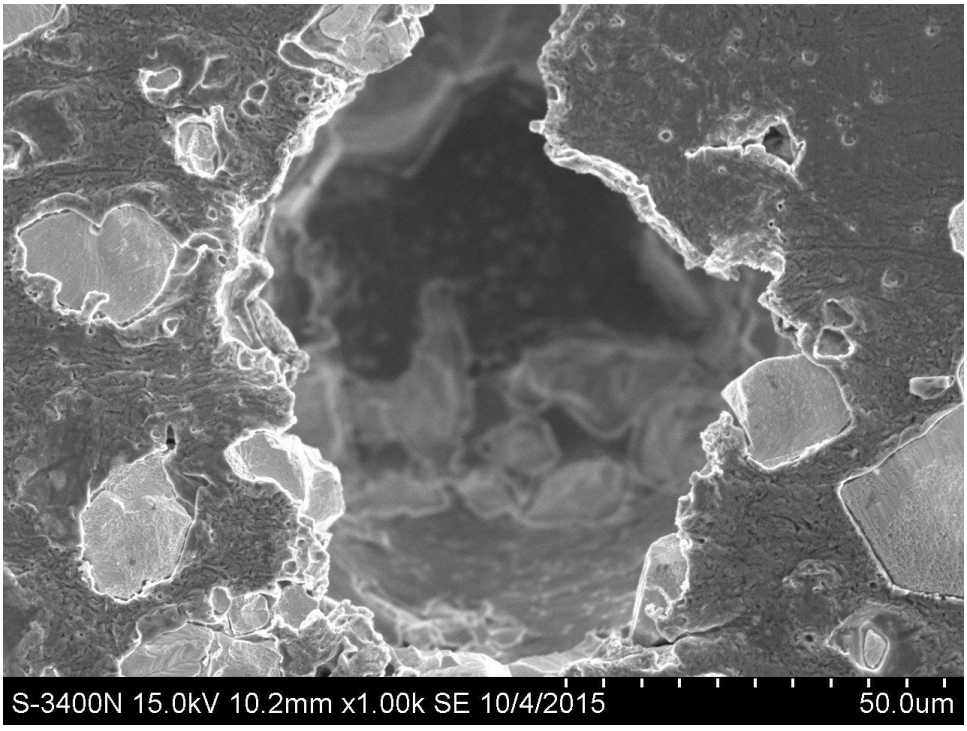

(d)

Fig. 14. Morphologies of corroded surface of LA-W-Cu-p1.8 after immersion test in SAR for different time: (a) 1 week; (b) 3 weeks; (c) 6 weeks; and (d) 9 weeks.

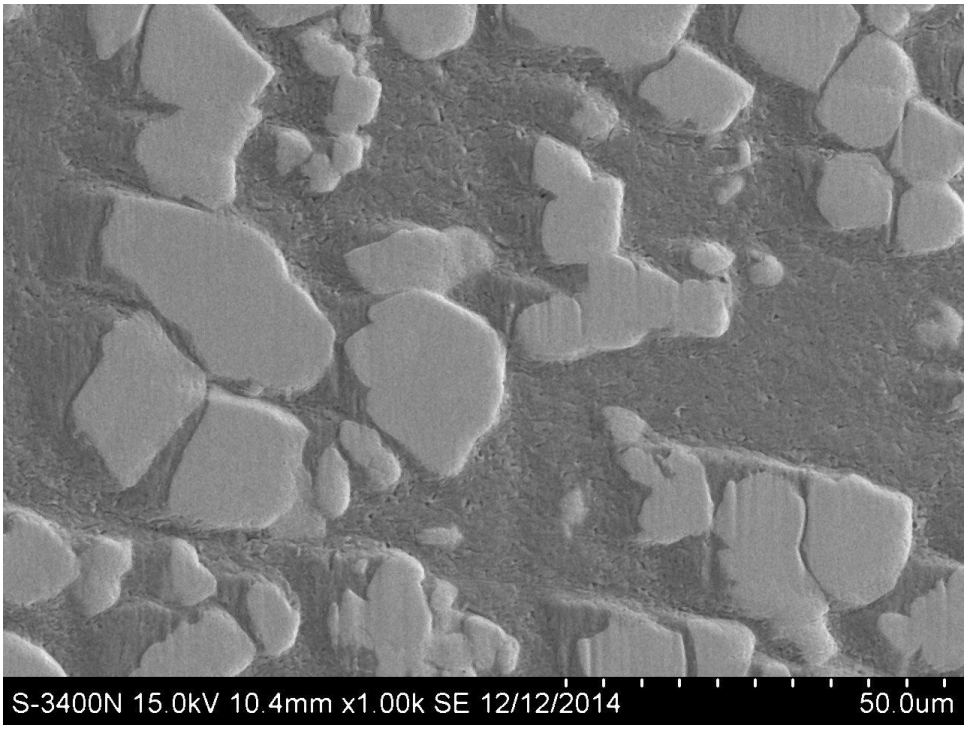
S-3400N 15.0kV 10.4mm x1.00k SE 12/12/2014
50.0um

(a)

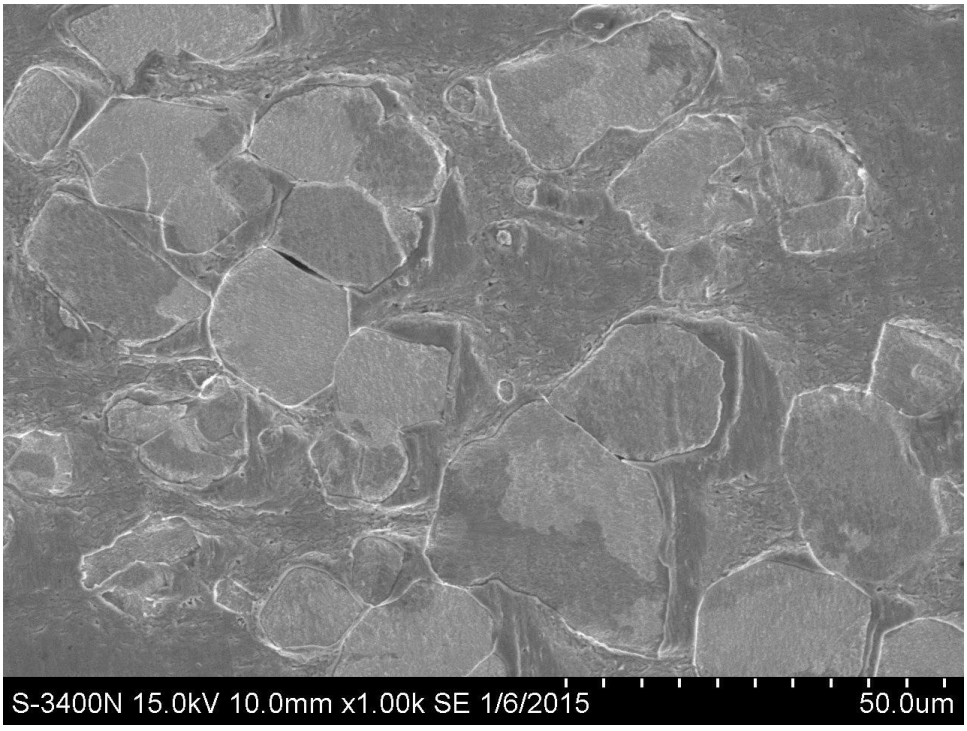
S-3400N 15.0kV 10.0mm x1.00k SE 1/6/2015
50.0um

(b)

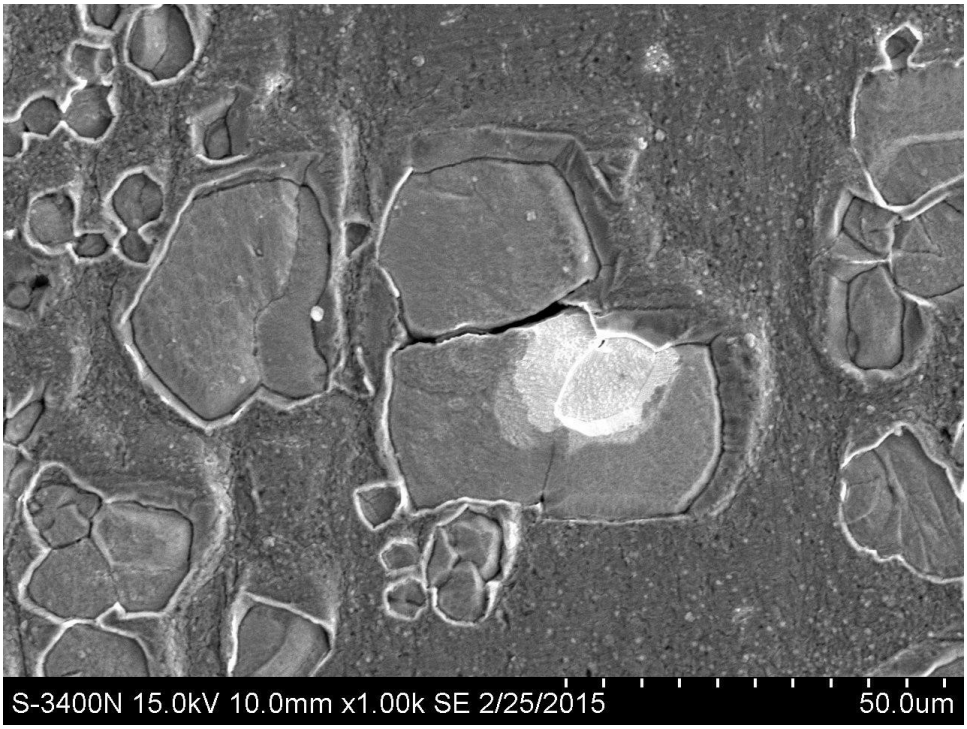

(c)

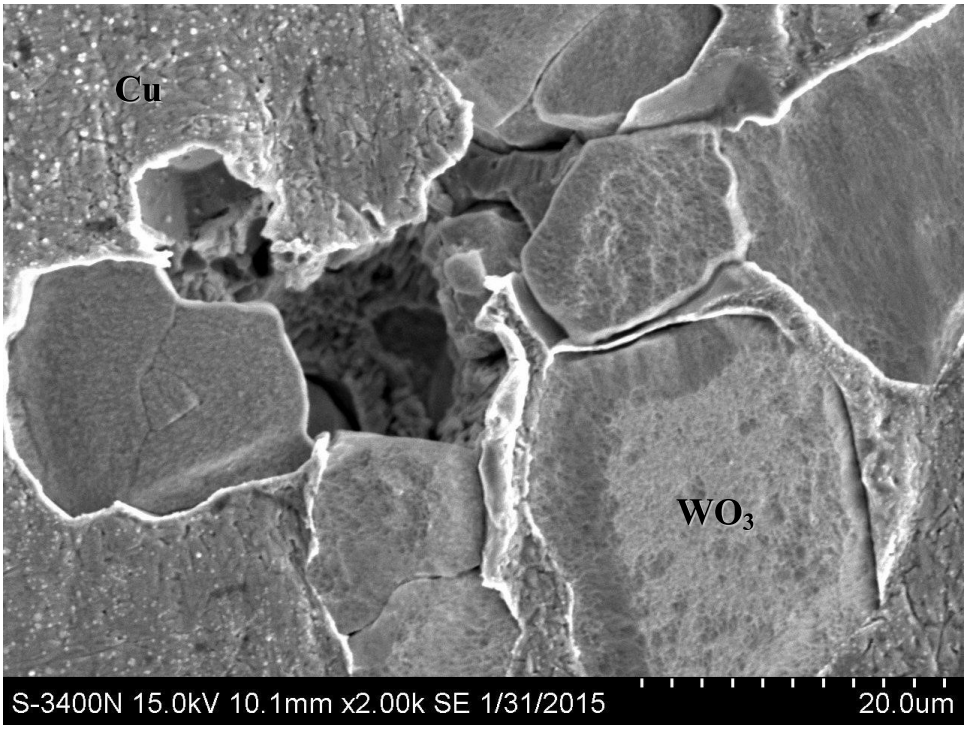

(d)

Fig. 15. Morphologies of corroded surface of LA-W-Cu-p2 after immersion test in SAR for different time: (a) 1 week; (b) 3 weeks; (c) 6 weeks; and (d) 9 weeks.

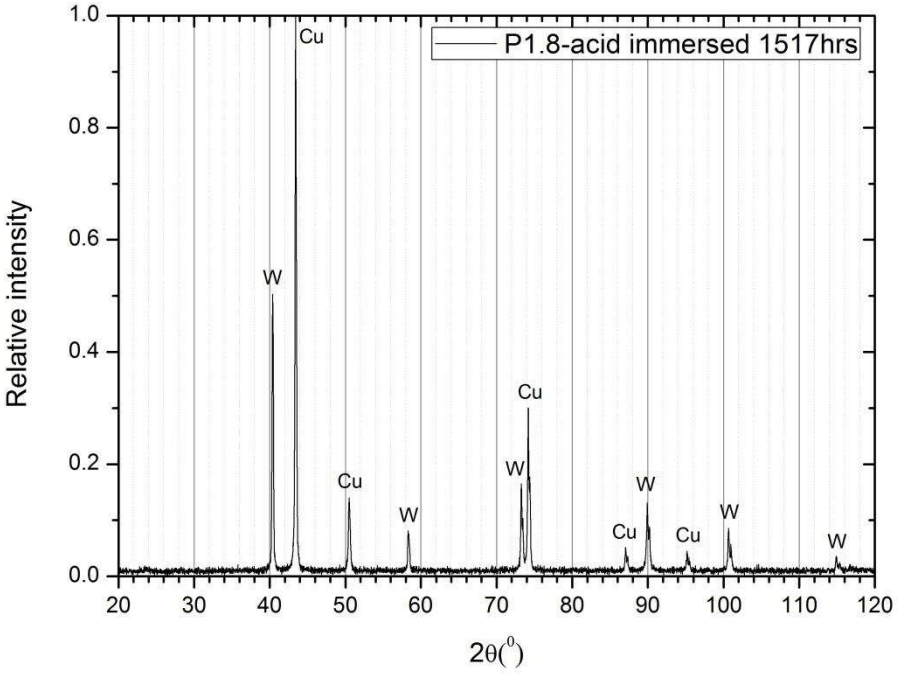

(a)

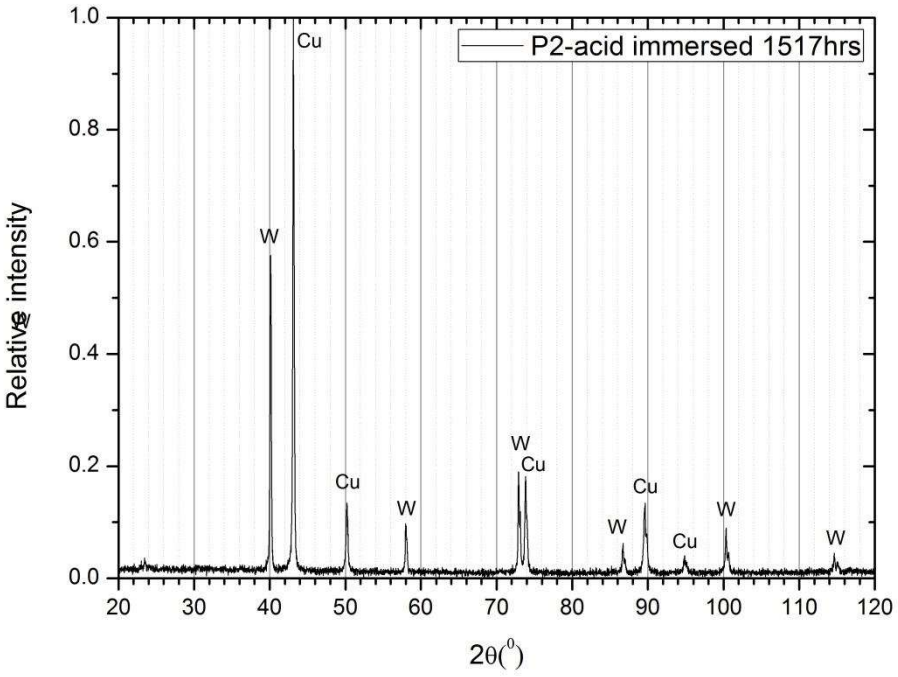

(b)

Fig. 16. XRD patterns of corroded surface of (a) LA-W-Cu-p1.8 and (b) LA-W-Cu-p2 in SAR.

Legends of Figures

Fig. 1. SEM micrographs of morphology of (a) Cu and (b) W powders.

Fig. 2. Laser-fabricated specimen LA-W-Cu-p1.8 showing (a) cross-sectional view; and (b) Cu matrix embedded with W particles.

Fig. 3. Laser-fabricated specimen LA-W-Cu-p2 showing (a) cross-sectional view; (b) Cu matrix embedded with W particles; and (c) EDX line scan across the W and Cu phases.

Fig. 4. XRD pattens of (a) LA-W-Cu-p1.8 and (b) LA-W-Cu-p2.

Fig. 5. (a) Plot of OCP vs time and (b) potentiodynamic polarization curves of the laser-fabricated specimens, cp Cu and cp W in 3.5% wt% NaCl solution at 25 ^{o}C.

Fig. 6. (a) Plot of OCP vs time and (b) potentiodynamic polarization curves of the laser-fabricated specimens, cp Cu and cp W in synthetic acid rain (SAR) at 25 ^{o}C

Fig. 7. Morphologies of corroded surface of cp Cu after immersion test in 3.5 wt% NaCl solution for different time: (a) 1 week; (b) 3 weeks; (c) 6 weeks; and (d) 9 weeks.

Fig. 8. Morphologies of corroded surface of cp W after immersion test in 3.5 wt% NaCl solution for different time: (a) 3 weeks; and (b) 9 weeks.

Fig. 9. Morphologies of corroded surface of LA-W-Cu-p1.8 after immersion test in 3.5 wt% NaCl solution for different time: (a) 1 week; (b) 3 weeks; (c) 6 weeks; and (d) 9 weeks.

Fig. 10. Morphologies of corroded surface of LA-W-Cu-p2 after immersion test in 3.5 wt% NaCl for different time: (a) 1 week; (b) 3 weeks; (c) 6 weeks; and (d) 9 weeks.

Fig. 11. XRD patterns of corroded surface of (a) LA-W-Cu-p1.8 and (b) LA-W-Cu-p2 in 3.5 wt% NaCl solution.

Fig. 12. Morphologies of corroded surface of cp Cu after immersion test in SAR for 9 weeks.

Fig. 13. Morphologies of corroded surface of cp W after immersion test in SAR for different time: (a) 3 weeks; and (b) 9 weeks.

Fig. 14. Morphologies of corroded surface of LA-W-Cu-p1.8 after immersion test in SAR for

different time: (a) 1 week; (b) 3 weeks; (c) 6 weeks; and (d) 9 weeks.

Fig. 15. Morphologies of corroded surface of LA-W-Cu-p2 after immersion test in SAR for different time: (a) 1 week; (b) 3 weeks; (c) 6 weeks; and (d) 9 weeks.

Fig. 16. XRD patterns of corroded surface of (a) LA-W-Cu-p1.8 and (b) LA-W-Cu-p2 in SAR.